






Binding zero modes with fluxons in Josephson junctions of time-reversal invariant topological superconductors

Gabriel F. Rodríguez Ruiz ¹, Adrian Reich ², Alexander Shnirman ^{2,3}, Jörg Schmalian ^{2,3} and Liliana Arrachea ^{1,4}

¹*Escuela de Ciencia y Tecnología and ICIFI, Universidad Nacional de San Martín-UNSAM, Av 25 de Mayo y Francia, 1650 Buenos Aires, Argentina*

²*Institute for Theory of Condensed Matter, Karlsruhe Institute of Technology (KIT), 76131 Karlsruhe, Germany*

³*Institute for Quantum Materials and Technologies, Karlsruhe Institute of Technology (KIT), 76131 Karlsruhe, Germany*

⁴*Centro Atómico Bariloche and Instituto de Nanociencia y Nanotecnología CONICET-CNEA (8400), San Carlos de Bariloche, Argentina*

We study the joint dynamics of the phase bias ϕ and the propagating Majorana fermions of the edge modes in Josephson junctions containing two-dimensional time-reversal invariant topological superconductors (TRITOPS). We consider TRITOPS-TRITOPS junctions, as well as junctions between topological and nontopological superconductors (TRITOPS-S). Both types of junctions are described by effective Dirac Hamiltonians with a ϕ -dependent mass. We analyze the effect of the phase fluctuations in the junction, as well as solitonic solutions of ϕ generated by fluxons trapped in the junction. We show that these solitons generate a spatial-dependent mass with a sign change akin to the Jackiw-Rebbi model. This enables the formation of zero-energy fermionic states localized at the fluxon. For the TRITOPS-TRITOPS junction these consist of a Kramers pair of Majorana modes, while for the TRITOPS-S one, there is a single Majorana fermion. The localized bound states hybridize in soliton-antisoliton configurations. Depending on the occupation state, these modes generate an effective attraction or repulsion in the dynamics of the soliton-antisoliton collision.

I. INTRODUCTION

The search for Majorana zero modes is one of the most active avenues of research in condensed matter physics. This is motivated by the relevance of topological properties of quantum matter [1,2] and because of the potential use of these quasiparticles as building blocks of fault-tolerant quantum computation [3,4]. One-dimensional (1D) topological superconductors host these quasiparticles localized at the ends. Several platforms to realize this phase have been proposed, including quantum wires [5–11], magnetic impurities [12–14], nontopological superconductors in proximity to topological insulators [15], and planar Josephson junctions controlled by the phase bias [16–22]. In two-dimensional (2D) systems the topological superconductors host chiral Majorana modes propagating along the edges. Promising signatures of these modes have been observed in iron-based compounds [23,24] and van der Waals heterostructures [25]. These and other results have been reviewed in Refs. [26–29].

A different class of topological superconductors exist that preserve time-reversal symmetry. These belong to the DIII class defined in Ref. [30] and are often referred to as TRITOPS (time-reversal invariant topological superconductors) [31]. There are many proposals to realize this topological phase in 1D and 2D systems [24,32–49]. The edge states of these topological superconductors appear in Kramers pairs and give rise to interesting physical properties like fractional spin densities and unusual features in the Josephson effect [39,50–66].

Recently, Josephson junctions with two-dimensional TRITOPS were studied in Ref. [67]. The edge states of 2D TRITOPS are Kramers pairs of counterpropagating helical Majorana modes. These modes can be effectively described by a Dirac Hamiltonian of neutral fermions, i.e., a Majorana Hamiltonian, where the hybridization at the Josephson junction defines, depending on the nature of the junction, up to two masses $m_1(\phi)$ and $m_2(\phi)$. These mass terms depend on the phase bias ϕ . Interestingly, when the junction is formed between a TRITOPS and a time-reversal invariant nontopological superconductor (S), the behavior of $m_2(\phi)$ is such that a quantum phase transition to a state with spontaneously broken time-reversal symmetry at the junction is possible. In this symmetry-broken state the equilibrium value of the phase takes values $\phi \neq n\pi$ with n integer. The consequence of such an instability is a peculiar behavior of the Josephson current $J(\phi)$ for small ϕ , while satisfying the condition $J(0) = 0$, dictated by time-reversal symmetry. Interestingly, a similar phenomenon takes place in the context of topological Josephson junctions with an embedded magnet. Here, the mass term is generated by the magnetization and a phase transition is predicted to take place when the fluctuations of the magnetic moment are taken into account [68]. One of the goals of this paper is the analysis of the fluctuations of ϕ in the TRITOPS-S junction and the stability of the state with broken time-reversal symmetry.

The second goal is to analyze the effect of vortices in the junction (fluxons). In S-S Josephson junctions, the dynamics of the phase bias is described by the sine-Gordon equation of motion and the fluxons lead to the formation of solitons (kink

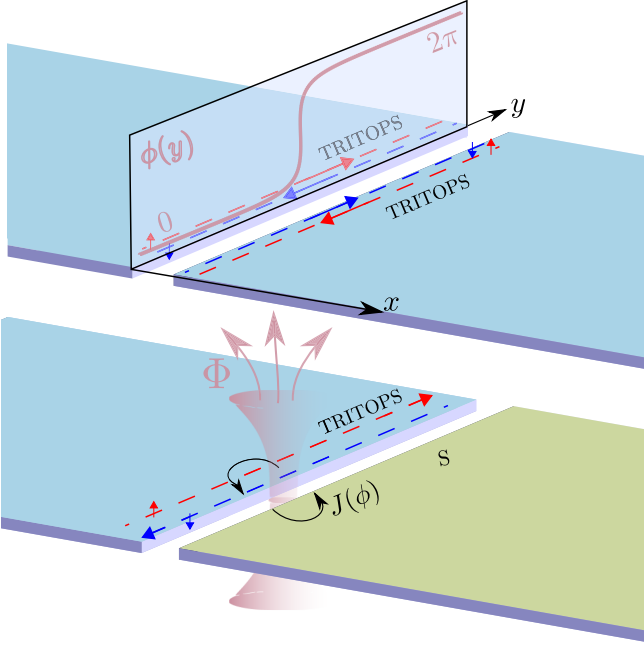


FIG. 1. Sketch of a TRITOPS-TRITOPS junction (top) with a soliton profile for the phase $\phi = 2\pi/\Phi_0$ and a TRITOPS-S junction (bottom) with a fluxon with flux Φ .

solutions of this equation) where the phase changes by 2π in the neighborhood of the fluxon [69–75]. This profile can propagate along the junction and can collide with other solitons traveling in the opposite direction. We show that the phase dynamics in the TRITOPS-TRITOPS junction can be described in a similar way. Instead, the TRITOPS-S junction is governed by a double sine-Gordon equation [76] and a double-kink solution represents a total change of 2π in the phase. In long Josephson junctions of 2D topological superconductors with broken time-reversal symmetry, the coupling between the solitons and the propagating Majorana edge states has been found to localize a Majorana zero mode at the fluxon [77]. A similar type of effect is also found to take place in planar Josephson junctions with magnetic field and spin-orbit coupling hosting a 1D topological superconducting phase [22].

We analyze the impact of single solitons and kink-antikink profiles in TRITOPS-S as well as TRITOPS-TRITOPS junctions. These generate sign changes in the mass terms of the effective Hamiltonian, describing Majorana modes of these junctions (see Fig. 1). Such a scenario defines an effective Jackiw-Rebbi model [78,79], which is known to have a localized zero mode. We show that the nature of the zero mode depends on the type of junction. In the TRITOPS-S junction the solitonic solutions are consistent with fractional fluxons that bind Majorana zero modes. The fluxons in the TRITOPS-TRITOPS junction also bind zero modes, which appear in Kramers pairs. In the case of kink-antikink profiles in the phase, these localized modes hybridize when they become sufficiently close to one another. Consequently, their energy becomes finite and this effect plays a role in the collisions. In fact, while ordinary kink and antikink cross one another in a collision [69], the finite energy of the hybridized modes

generates an effective repulsion or attraction, which should affect that behavior.

The paper is organized as follows. We present the effective description to analyze the joint dynamics of the phase bias and the Majorana edge modes at the different types of Josephson junctions in Sec. II. Section III is devoted to analyzing the stability of the mean-field description in the TRITOPS-S junction. The equation of motion for the phase and the corresponding solitonic solutions in the different junctions are analyzed in Sec. IV, while Sec. V is devoted to study the type of electronic bound states which are generated by these solitonic profiles in the phase. The impact of the electron bound states in the collision of solitons is discussed in Sec. VI. A summary and conclusions are presented in Sec. VII. Some technical details are presented in the Appendixes.

II. DESCRIPTION OF THE JUNCTION

We consider the following effective action, which describes the joint dynamics of the phase bias along the junction $\phi = 2\pi\Phi/\Phi_0$ ($\Phi_0 = h/2e$), and its coupling to the TRITOPS' edge modes: $S = S_\phi + S_{\eta-\phi}$. These two components read as

$$S_\phi = \int_{y,t} \left\{ \frac{\hbar K}{2} \left(\frac{1}{c_J} (\partial_t \phi)^2 - c_J (\partial_y \phi)^2 \right) - E_J (1 - \cos \phi) \right\} \quad (1)$$

as well as

$$S_{\eta-\phi} = \frac{1}{2} \int_{y,t} \eta^\dagger (i\hbar \partial_t - \mathcal{H}) \eta, \quad (2)$$

with Dirac Hamiltonian

$$\mathcal{H} = -i\hbar v \alpha \partial_y + m_1(\phi) \beta_1 + m_2(\phi) \beta_2. \quad (3)$$

We use the notation $\int_{y,t} \dots = \int dy dt \dots$. The precise expressions for the matrices α and $\beta_{1,2}$ depend on the nature of the junction and will be given below. S_ϕ describes the dynamics of the phase, taking into account the effect of the states above the gap only. E_J is the Josephson energy density per length, which is related to the amplitude of the Josephson current density (per length) $J(\phi) = J_0 \sin(\phi)$ via $J_0 = 2eE_J/\hbar$.

The gradient contributions to S_ϕ originate in the energies of the electric and magnetic fields. The action assumed here corresponds to a three-dimensional (3D) situation, i.e., a junction of sufficiently large height $h_z \gg \lambda_{1,2}$, where $\lambda_{1,2}$ are the respective London penetration depths. In this regime the junction forms a wave guide with most of the magnetic and electric energies bound to its volume. The phase rigidity K and the effective light velocity (Swihart velocity) c_J are then determined by the geometry of the junction and given by $c_J^2 = c^2 d_0/d$, $K = \hbar c h_z / (16\pi e^2 \sqrt{d d_0})$. Here d_0 is the width of the insulating barrier separating the two superconductors and $d = d_0 + \lambda_1 + \lambda_2$ [80]. If h_z becomes too small, $h_z \ll \lambda_{1,2}$, stray magnetic fields extending outside of the junction need to be considered, leading to a nonlocal effective action [81].

Although the effective models for the topological superconductors considered in the present work are 2D, the mechanisms to generate such phases are typically by proximity to 3D superconductors [24,31,32,35,38–42,44,45,49]. We assume these 3D superconductors to provide the necessary

suppression of the stray magnetic fields through their height h_z , acting as a wave guide and allowing us to consider a purely local theory. Note that in the usual 3D Josephson junctions the Josephson energy density E_J per length is also proportional to h_z [80,82]. In that case, one introduces the Josephson energy density per area so that the height h_z becomes a prefactor of the whole action S_ϕ , which can effectively be reformulated such that K is the prefactor of S_ϕ . In contrast, here the Josephson tunneling takes place only between the 2D superconducting layers, thus, our Josephson energy density per length E_J is completely unrelated to K .

$S_{\eta-\phi}$ describes the coupling between the Majorana edge states and the phase. The details depend on the type of junction, which is characterized by the mass terms $m_{1,2}(\phi)$ and the number of Kramers pairs of counterpropagating Majorana modes involved. The latter defines the structure of the spinor η (see Ref. [67]). v is the velocity of the Majorana modes.

In the action introduced in Eqs. (1)–(3) we consider two mass terms. The first one is denoted by $m_1(\phi)\beta_1$ and corresponds to a coupling between the edge modes on both sides of the junction. Its leading contribution is of first order in the tunneling element t_J . The second mass term in Eq. (3), denoted by $m_2(\phi)\beta_2$, is due to the virtual coupling of edge modes on one side of the junction to states above the gap on the other side. Hence, it effectively couples the edge modes within each superconductor and is of order $t_J^2/\Delta_{\text{eff}}$ with Δ_{eff} being the magnitude of the superconducting gap. Obviously, for the TRITOPS-S junction m_2 is the only possible mass term.

We now summarize the description on the basis of low-energy Hamiltonians describing a spin-preserving tunneling (t_J) at the Josephson junction, following the derivation presented in Ref. [67]. For the TRITOPS-S junction there is a single pair of counterpropagating Majorana modes (see Fig. 1). Consequently, η is a two-component spinor and we have

$$\alpha = \sigma^z, \quad \beta_2 = \sigma^y, \quad (4)$$

$$m_1(\phi) = 0, \quad m_2(\phi) = m_2^{(0)} \sin(\phi). \quad (5)$$

(TRITOPS-S).

The Pauli matrices σ act on the two members of the Majorana Kramers pair. The edge modes of the TRITOPS are coupled to the supragap states of the nontopological superconductor S. As mentioned before, the nonvanishing mass term $m_2^{(0)} \propto t_J^2/\Delta_{\text{eff}}$ is originated in a second-order process in the tunneling amplitude.

In distinction, for the TRITOPS-TRITOPS junction (also sketched in Fig. 1), η is a spinor with four components corresponding to the two Kramers pairs associated to the two TRITOPS (labeled by S_1, S_2), and we have

$$\alpha = \tilde{\sigma}^z \sigma^z, \quad \beta_1 = \tilde{\sigma}^y \sigma^z, \quad \beta_2 = \tilde{\sigma}^0 \sigma^y, \quad (6)$$

$$m_1(\phi) = m_1^{(0)} \cos(\phi/2), \quad m_2(\phi) = m_2^{(0)} \sin(\phi) \quad (7)$$

(TRITOPS-TRITOPS).

$\tilde{\sigma}^j$ are Pauli matrices acting in the S_1, S_2 subspace while σ^j act on the two partners of the Kramers pair. Here, the mass term modulated by $m_1^{(0)} \propto t_J$ is generated by the hybridization of the Majorana edge states at both sides of the junction. This

is the leading order in the tunneling t_J and it is exact when the superconducting gap is large enough $\Delta_{\text{eff}} \gg t_J$ to prevent the hybridization of the edge modes on one side of the junction with the supragap states of the other side. The second mass term $m_2(\phi)$ is a second-order perturbation with $m_2^{(0)} \propto t_J^2/\Delta_{\text{eff}}$ and has to be taken into account when the edge states on one of the TRITOPSs hybridize, not only with the edge states, but also with the supragap states of the other TRITOPS.

To identify the 4×4 matrices α and $\beta_{1,2}$ of Eq. (6) that determine the Dirac Hamiltonian \mathcal{H} for the TRITOPS-TRITOPS junction, we analyze the behavior under time reversal, charge conjugation, and under the exchange of the two identical TRITOPSs. Time reversal corresponds to simultaneously transforming $\phi \rightarrow -\phi$ and $\mathcal{T} = i\tilde{\sigma}^0 \sigma^y \mathcal{K}$ in the fermion sector. The charge-conjugation operator $C = U_C \mathcal{K}$ acts on the BdG Hamiltonian as $U_C \mathcal{H} U_C^{-1} = -\mathcal{H}^*$. We use a basis with real field operators $\eta^\dagger = \eta$. In this basis $U_C = 1$ and thus $\mathcal{H} = -\mathcal{H}^*$. Finally, the exchange symmetry of the two superconductors S_1 and S_2 corresponds to simultaneously transforming $\phi \rightarrow -\phi$ and $U_X = \tilde{\sigma}^x \sigma^x$ in the fermion sector. The conditions of time reversal, charge conjugation, and exchange symmetry uniquely determine the matrices for the TRITOPS-TRITOPS junction. In Appendix B we give further details on the derivation of these symmetries. The underlying assumptions are p_\pm type of pairing in both superconductors and spin-preserving tunneling at the junction.

The transformation $\phi \rightarrow -\phi$ is necessary if the phase ϕ is a genuine dynamic variable. However, if one considers the properties of the fermionic sector for a fixed configuration $\phi(y)$, the mass term $m_2(\phi)$ breaks both the time-reversal and the exchange symmetry. This will be important when we analyze the fermionic spectrum near given soliton solutions of the phase.

The distinct dependency of the edge-mode mass $m_{1,2}(\phi)$ for the two junctions, given in Eqs. (5) and (7), gives rise to qualitatively distinct behavior. For the TRITOPS-TRITOPS junction, the net mass at $\phi = 0$ is finite while it vanishes for the TRITOPS-S junction. This is consistent with the bulk-boundary correspondence; see Ref. [67] for a discussion. As we will see, a fermion zero mode will only be associated with a phase-slip soliton if the fermion is massive at constant phase. For the TRITOPS-S, this requires spontaneously breaking time-reversal symmetry with an equilibrium phase $\phi \neq n\pi$. In this case, the protecting symmetry of the massless edge modes is spontaneously broken for the TRITOPS-S junction and the bulk-boundary correspondence does not apply. We will see below that the stability of the time-reversal symmetry-broken state depends on the value of the rigidity K . The symmetry is broken for large values of K and hence large values of h_z , while at small K quantum fluctuations are important and restore the symmetry. The ordered state is characterized by an Ising variable that describes the two states $\pm \tilde{\phi} \bmod(2\pi)$. The quantum phase transition is then expected to be in the tricritical Ising universality class [83,84], the natural transition from an Ising ordered phase to a massless, critical phase that corresponds to the critical point in the usual Ising model. It is described by the tricritical Ising conformal field theory with central charge $7/10$. In our analysis we are more interested in the quantitative location and parameter dependence of this transition and in the properties of phase slips on the ordered

side of the transition. The ordered state can be described in a controlled fashion in the limit of large rigidity K . To estimate the phase boundary we will then go beyond the mean-field limit, valid at $K \rightarrow \infty$, and include fluctuation effects; the transition is then estimated from the parameter regime where these fluctuations start to dominate the equation of state.

III. LARGE PHASE RIGIDITY AND ROLE OF FLUCTUATIONS

We now consider a semiclassical approach, where the fermionic modes are treated in a full quantum mechanical framework, while $\phi(y, t)$ is regarded as a classical field defined by its mean value with $K \rightarrow \infty$ in Eq. (1). Under this assumption, we express $\eta(y) = \sum_k e^{iky} \eta_k$ and we consider the Hamiltonian in Eq. (3) where the masses $m_{1,2}(\phi)$ are functions of the classical field ϕ , specified in Eqs. (5) and (7). The total energy density after integrating out all the fermionic modes of the junction in $\langle H_{\eta-\phi} \rangle$ and adding the contribution of the supragap states reads as

$$E(\phi) = E_J[1 - \cos(\phi)] - \frac{m^2(\phi)}{8\pi\hbar v} \left[1 + \log \left(\frac{4\Lambda^2}{m^2(\phi)} \right) \right], \quad (8)$$

where $m^2(\phi) = m_1^2(\phi) + m_2^2(\phi)$ is the net mass and Λ a high-energy cutoff of the order of the effective superconducting gap Δ_{eff} .

The contribution of the states above the superconducting gap, i.e., all states except for the edge modes, is given by the first term of Eq. (8) which has a minimum at $\phi = 0$. As discussed above, the effect of the edge modes given by the second term does not affect this minimum in the TRITOPS-TRITOPS junction since $m(\phi) \propto m_0$ at small ϕ , while a competing minimum may develop for the TRITOPS-S junction [67]. In what follows we analyze the stability of this time-reversal symmetry-breaking solution in the TRITOPS-S junction against the effect of the phase fluctuations introduced by a finite K in Eq. (1).

Under the assumption $\phi \ll 1$, one finds the minima of the ground-state energy density (8) to be

$$\phi_{\text{eq}}^{(1/2)} = \pm \frac{2\Lambda}{m_0} \exp \left(-\frac{\pi\hbar v E_J}{m_0^2} \right) \neq 0, \quad (9)$$

hinting, as discussed, at a spontaneous symmetry breaking. However, one has to keep in mind the possibility of quantum fluctuations of ϕ destroying the phase with $\phi_{\text{eq}} \neq 0$. This is exemplified by expanding the action in Eq. (1) up to second order in ϕ , which yields the Gross-Neveu-Yukawa (GNY) model in 1+1 dimensions, a bosonized version of the Gross-Neveu model [85] $S \approx S_\phi^{(0)} + S_{\eta-\phi}$ with

$$S_\phi^{(0)} = \int_{y,t} \left\{ \frac{\hbar K}{2} \left(\frac{1}{c_J} (\partial_t \phi)^2 - c_J (\partial_y \phi)^2 \right) - \frac{E_J}{2} \phi^2 \right\}. \quad (10)$$

In the limit $K \rightarrow 0$, integrating out ϕ results in a local 4-Majorana interaction which is renormalization-group (RG) irrelevant and thus no symmetry breaking takes place: in this limit, the mean-field approach is invalidated by fluctuations. Since the stiffness K suppresses the fluctuations (and renders the effective 4-Majorana interaction nonlocal), we expect a

quantum phase transition at some positive value of K , beyond which the nonzero expectation value of ϕ is stabilized.

While in the GNY model the question regarding a symmetry-broken phase poses a strong-coupling problem, formally not accessible via perturbative methods, it has been shown in Ref. [68] that one can derive an estimate for the parameter regime in which symmetry breaking is allowed by analyzing the corrections to the equation of state $dE(\phi)/d(\phi^2) = 0$ due to Gaussian fluctuations.

Following the reasoning of Ref. [68], we expand the GNY action up to second order in the fluctuations $\delta\phi$ around some assumed minimum $\langle \phi \rangle = \tilde{\phi}$ of the ground-state energy $\phi(x, t) = \tilde{\phi} + \delta\phi(x, t)$. After integrating out $\delta\phi$, we derive the equation of state for $\tilde{\phi}$ and examine whether it allows for solutions $\tilde{\phi} \neq 0$, i.e., whether the mean-field solution is consistent and only weakly affected by fluctuations. If this is the case, we conclude that fluctuations are small and the treatment in the limit of large rigidity therefore justified. If not, fluctuations are large, suppress long-range order, and the symmetry remains unbroken.

The fluctuation-corrected equation of state determining the gap in the Majorana spectrum, the derivation of which is sketched in Appendix C, reads as

$$\frac{dE}{d(\tilde{\phi}^2)} = 0 \quad \Leftrightarrow \quad \log \left| \frac{\tilde{\phi}}{\phi_{\text{eq}}} \right| + \chi_{\tilde{\phi}} = 0, \quad (11)$$

with

$$\begin{aligned} \chi_{\tilde{\phi}} = & \frac{4}{\pi} \int_0^{\pi/2} d\theta \int_0^\infty dr \frac{\text{Arsinh}(r)}{\sqrt{1+r^2}} \\ & \times \left[8\pi K \tilde{\phi}^2 r^2 \left(\frac{v}{c_J} \sin^2 \theta + \frac{c_J}{v} \cos^2 \theta \right) \right. \\ & \left. + \log \left| \frac{\tilde{\phi}}{\phi_{\text{eq}}} \right| + \frac{\sqrt{1+r^2}}{r} \text{Arsinh}(r) \right]^{-1}. \end{aligned} \quad (12)$$

Here, (r, θ) are polar coordinates in the $(\frac{\hbar\omega}{2m_0\tilde{\phi}}, \frac{\hbar vq}{2m_0\tilde{\phi}})$ plane. We calculate the integral numerically for different values of v/c_J and find the curve of critical values $\Gamma_c(v/c_J)$ depicted in Fig. 2, representing the minimum value $K\phi_{\text{eq}}^2$ needs to take on in order for solutions to Eq. (11) to exist and thus the symmetry breaking to be stable against Gaussian fluctuations. The relevant experimental scenario corresponds to small values of $v/c_J \ll 1$ ($\simeq 10^{-4}$ – 10^{-3}), in which case a small value of $K\phi_{\text{eq}}^2$ is enough to guarantee the stability of the mean-field solution. The precise value of K should anyway depend on the geometric details of the junction.

Within the Gaussian fluctuation framework, the quantum phase transition is of first order. However, there is no reason to expect that the employed approximation properly describes the critical fluctuations at this transition correctly. As stated above, the quantum phase transition is expected to be in the tricritical Ising universality class, where all exponents are exactly known. Our approach is, however, very useful in getting an estimate of the phase boundary as function of the system parameters.

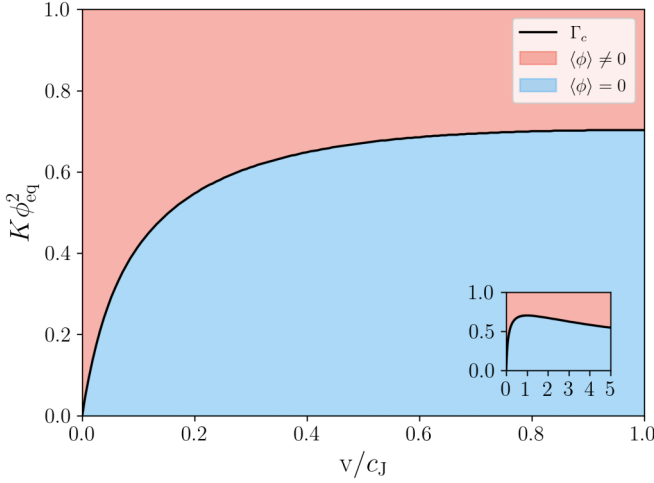


FIG. 2. Phase diagram of the TRITOPS-S junction with the boundary Γ_c between symmetry-broken (red) and -unbroken (blue) phase determined from Eq. (11) for $v/c_J \in [0, 1]$ (inset: $v/c_J \in [0, 5]$).

IV. EQUATION OF MOTION FOR THE PHASE BIAS AND SOLITONIC SOLUTIONS

We now focus on the regime of large K of Fig. 2, where the fluctuations of the phase bias are not dominant so that we can regard $\phi(y, t)$ as a classical variable leading to a current-phase relation (CPR) $J(\phi)$. We assume that the length of the junction is significantly larger than the Josephson penetration depth of the two superconductors λ_1, λ_2 . Hence, the phase may have a spatial dependence along the junction which is represented by $\phi(y, t)$, whose dynamics is described by the following equation of motion:

$$\frac{\hbar}{2e} C \partial_t^2 \phi - \frac{\hbar}{2e} \frac{1}{L} \partial_y^2 \phi + J(\phi) = -\frac{\hbar G_N}{2e} \partial_t \phi + J_{\text{ext}}. \quad (13)$$

Here, $C = h_z/(4\pi d_0)$ and $L = 4\pi d/(h_z c)^2$ are the capacitance per length and the inductance per length of the wave guide, respectively. The right-hand side of the equation describes the dissipation due to the normal conductance (per length) G_N and the driving with an external current density J_{ext} .

The homogeneous equation corresponding to Eq. (13) with the right-hand side equal to zero defines the sine-Gordon equation [69] for $J(\phi) = J_0 \sin(\phi)$. This is the equation of motion derived from the action S_ϕ of Eq. (1). In fact, one can introduce new length scales and timescales, λ_J and ω_J^{-1} , and redefine $y/\lambda_J \rightarrow y$, $t\omega_J \rightarrow t$, such that the homogeneous equation simply reads as

$$\phi_{tt} - \phi_{yy} + \sin \phi = 0. \quad (14)$$

It admits soliton, or kink, solutions associated to fluxons trapped in the junction [69]. These solutions have the following structure:

$$\phi(y, t) = 4 \arctan \left(e^{\frac{y-ut}{\sqrt{1-u^2}}} \right), \quad (15)$$

being u the velocity at which the soliton propagates. Its precise value is determined by considering the full Eq. (13), including the right-hand side.

We now focus on the static limit of Eq. (13) in the homogeneous case ($u = 0$) and we defer the discussion of the dynamical effects to Sec. VI. Expressing the CPR as $J(\phi) = E_J \partial_\phi \epsilon(\phi)$, this equation can be written as

$$\frac{1}{2} \frac{d}{dy} \left(\frac{d\phi}{dy} \right)^2 = \frac{d\epsilon(\phi)}{dy}. \quad (16)$$

Taking into account the boundary conditions $d\phi(y)/dy = 0$, $y \rightarrow -\infty$ and $\phi(y) = \phi_{\text{eq}}$, $y \rightarrow \infty$, being ϕ_{eq} the phase corresponding to the minimum of $\epsilon(\phi)$, Eq. (16) can be also expressed as

$$\frac{d\phi}{dy} = \pm \sqrt{2\delta\epsilon(\phi)}, \quad \delta\epsilon(\phi) = \epsilon(\phi) - \epsilon(\phi_{\text{eq}}). \quad (17)$$

It is easy to verify that for $\epsilon(\phi) = 1 - \cos(\phi)$, we recover the stationary sine-Gordon equation with the solution given by Eq. (15).

Our aim is to solve Eq. (16) for different configurations of Josephson junctions containing one or two TRITOPSS.

A. TRITOPS-S junction

The remarkable feature of this junction is the fact that the phase corresponding to the minimum energy, ϕ_{eq} , has a finite value $0 < \phi_{\text{eq}} \leq \pi/2$, meaning a spontaneous symmetry breaking for arbitrarily small values of the phase bias.

In order to address the related properties of the junction, we focus on specific parameters in Eq. (8), which lead to an integrable double sine-Gordon equation [76] for the phase bias. This corresponds to assuming $\Lambda \gg m_0$ in Eq. (8), so that we can substitute the term with the logarithm function by a constant. The result is

$$E(\phi) \simeq E_J [1 - \cos(\phi)] - E_0 [1 - \cos(2\phi)]. \quad (18)$$

This energy has two minima at

$$\phi_{\text{eq}}^{(1)} = \phi_0, \quad \phi_{\text{eq}}^{(2)} = 2\pi - \phi_0, \quad \phi_0 = \arccos \left(\frac{E_J}{4E_0} \right). \quad (19)$$

We see from the definition of ϕ_0 that the two solutions, $\phi_{\text{eq}}^{(j)}$, $j = 1, 2$, exist provided that $4E_0 > E_J$. Otherwise, we get the single (usual) solution $\phi_{\text{eq}} = 0, \text{ mod}[2\pi]$. We benchmark this description against the numerical solution of a lattice model, where $E(\phi)$ is calculated in a junction between two BCS Hamiltonians defined in a square lattice connected in a Josephson arrangement following Ref. [67] (see details in Appendix A). One of the Hamiltonians (corresponding to the superconductor S_1) is a TRITOPS with p -wave and s -wave pairing, respectively. $\Delta_p^{(1)}$, $\Delta_s^{(1)}$, and chemical potential μ within the topological phase, where this system has propagating Majorana modes at the edges. The motivation for considering these two components of the pairing is the fact that many proposals for achieving the TRITOPS phase in real materials rely on a combination of s -wave superconductivity with spin-orbit coupling (see, for instance, Refs. [24,31,32,49,67]), which effectively induces p -wave and s -wave pairing. The model for the nontopological Hamiltonian has only s -wave pairing $\Delta_s^{(2)}$. In order to minimize finite-size effects, periodic boundary conditions are implemented along the direction y , parallel to the junction. The dimension of the lattice is $N_x = N_y = 300$ sites for each of

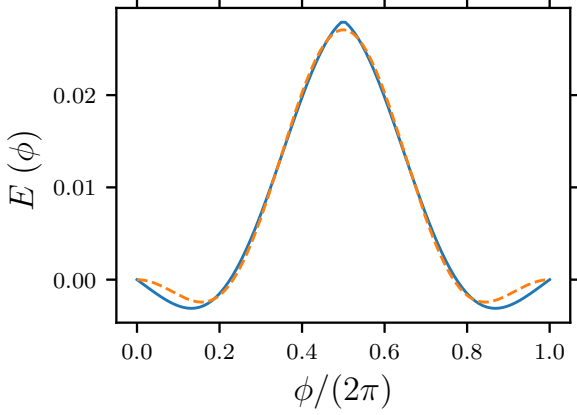


FIG. 3. Plot in continuous lines: Energy vs phase for a junction S_1 - $S_2 \equiv$ TRITOPS-S calculated in the lattice model defined in Appendix A with $N_x = N_y = 300$ sites and periodic boundary conditions along the junction. Parameters are the tunneling hopping at the junction $t_J = w/5$, the amplitude of the pairing potentials of the two superconductors, $\Delta_s^{(2)} = \Delta_p^{(1)} = 4\Delta_s^{(1)} = w/5$, and the chemical potential $\mu = -2w$, being w the hopping parameter of the square lattice. Plot in dashed lines: Eq. (18) with $E_0 = 0.006$ and $E_J = 0.014$.

the superconductors. The ground-state energy shown in Fig. 3 is calculated by adding all the negative single-particle energies of the Bogoliubov–de Gennes Hamiltonian. We clearly see two minima corresponding to $\phi_0 \neq 0$. The precise value depends on the model parameters, mainly on $\Delta_p^{(1)}$, $\Delta_s^{(1)}$. We compare these numerical results with those calculated from Eq. (18) with parameters E_0 and E_J optimized to fit the numerical data. A good agreement is found in the results shown in the figure. This supports Eq. (18) as a representative limit to analyze the phase dynamics of the TRITOPS-S junction.

We now turn to discuss the possibility of having solitonic solutions to Eq. (17) in this peculiar junction. We focus on the situation where we get the two minima given by Eq. (19) and we express $\delta\epsilon(\phi) = [E(\phi) - E(\phi_0)]/E_J$ as

$$\delta\epsilon(\phi) = -\cos(\phi) + \frac{1}{2\cos(\phi_0)}[\cos^2(\phi) + \cos^2(\phi_0)]. \quad (20)$$

This defines an integrable double sine-Gordon equation [76]. It has two solitonic solutions, which correspond to solving

$$s \int_{\phi_j}^{\phi_j} d\phi \frac{1}{\sqrt{2\delta\epsilon(\phi)}} = y - y_0, \quad (21)$$

with $s = \pm$, $\phi_1(y_0) = \bar{\phi}_1 = 0$, and $\phi_2(y_0) = \bar{\phi}_2 = \pi$. They read as

$$\begin{aligned} \phi_1(y) &= 2 \arctan \left[\tan \left(\frac{\phi_0}{2} \right) \tanh \left(\frac{|\sin \phi_0|}{2\sqrt{\cos(\phi_0)}} s(y - y_0) \right) \right], \quad -\phi_0 \leq \phi \leq \phi_0 \\ \phi_2(y) &= \pi - 2 \arctan \left[\tan \left(\frac{\phi_0 - \pi}{2} \right) \tanh \left(\frac{|\sin \phi_0|}{2\sqrt{\cos(\phi_0)}} s(y - y_0) \right) \right], \quad \phi_0 \leq \phi \leq 2\pi - \phi_0. \end{aligned} \quad (22)$$

Both solutions evolve between the two equilibrium phases and are shown in Fig. 4(a). Recalling that a change of 2π in the phase is associated to a flux quantum $h/(2e)$, we see that each of these solitons is associated to a fraction of the flux quantum.

Interestingly, the spatial dependence of the phase in these two solutions of the double sine-Gordon equation for the junction introduces important changes in the mass term of Eq. (3). In fact, substituting the functions $\phi_j(y)$ in $m_2(\phi)$, we find its dependence with the position along the junction. The results are shown in Fig. 4(b).

B. TRITOPS-TRITOPS junction

The equilibrium phase in this case is $\phi_{eq} = 0$. As before, we approximate Eq. (8) by substituting the logarithm by a constant, which results in $E(\phi) \simeq E_J - E_0/2 - (E_J + E_0/2)\cos(\phi)$. Therefore, $\delta\epsilon(\phi) = \frac{E(\phi) - E(0)}{E_J} \simeq (1 + \frac{E_0}{2E_J})[1 - \cos(\phi)]$ and Eq. (16) reads as

$$\int_{\pi}^{\phi} d\phi \frac{1}{\sqrt{2\delta\epsilon(\phi)}} = y - y_0, \quad (23)$$

being $\phi(y_0) = \pi$. The solution for a kink is

$$\phi(y) = 4 \arctan \left(e^{\sqrt{\frac{E_0}{2E_J} + 1}(y - y_0)} \right), \quad (24)$$

and it is shown in Fig. 5(a). We see that this kink solution is very similar to Eq. (15) but with a soliton width given by $a^{-1} = (\frac{E_0}{2E_J} + 1)^{-1/2}$.

Substituting in the mass from Eq. (6), we find the following behavior for its variation as a function of the position:

$$\begin{aligned} m_1(y) &= -m_1^{(0)} \tanh[a(y - y_0)], \\ m_2(y) &= -2m_2^{(0)} \tanh[a(y - y_0)] \sqrt{1 - \tanh^2[a(y - y_0)]}. \end{aligned} \quad (25)$$

For an antisoliton, the overall minus sign for both masses is replaced by a plus sign. The masses $m_{1,2}(y)$ as function of position are shown in Fig. 5. Both masses are odd under $y \rightarrow -y$, i.e., $m_{1,2}(-y) = -m_{1,2}(y)$. While $m_1(y \rightarrow \pm\infty) \rightarrow \mp m_1^{(0)}$, the mass $m_2(y)$ has support only near the soliton, i.e., $m_2(y \rightarrow \pm\infty) \rightarrow 0$.

V. ELECTRON BOUND STATES AT THE FLUXON

We now analyze the coupling between the phase and the fermions in the edge states when the junction has trapped fluxons, leading to the solitonic profiles discussed in the previous section, using the Hamiltonian in Eq. (3), where we recall that $\eta(y)$ are spinors collecting the members of the Kramers pair of the counterpropagating Majorana modes.

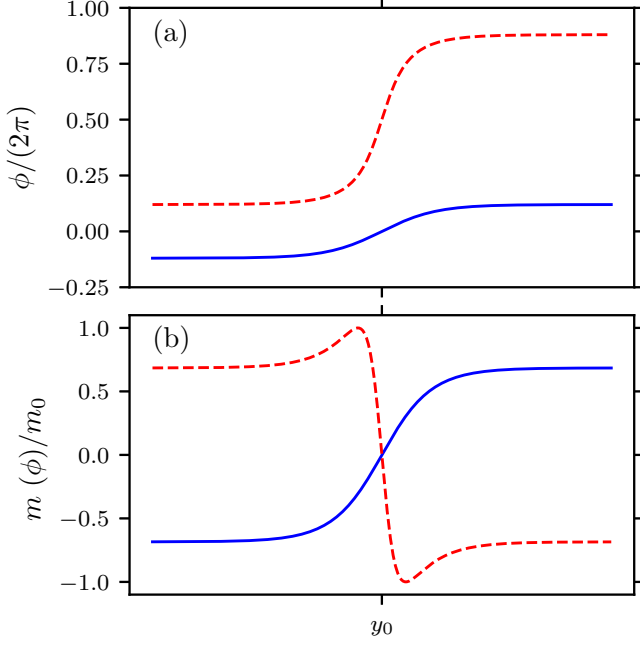


FIG. 4. Profile for a soliton of the phase (a) and the mass $m_2(\phi)$ (b) for the two types of solution ϕ_1 and ϕ_2 of the TRITOPS-S junction represented by continuous and dashed lines with $\phi_0 = 0.12 \times 2\pi$.

For the TRITOPS-S junction there is a single pair of Majorana modes (see Fig. 1) and we have

$$\eta(y) = (\eta_\uparrow(y), \eta_\downarrow(y))^T \quad (\text{TRITOPS-S}). \quad (26)$$

Instead, in the TRITOPS-TRITOPS junction this spinor has four components corresponding to the two Kramers pairs associated to the two TRITOPS (labeled by $j = 1, 2$), and we

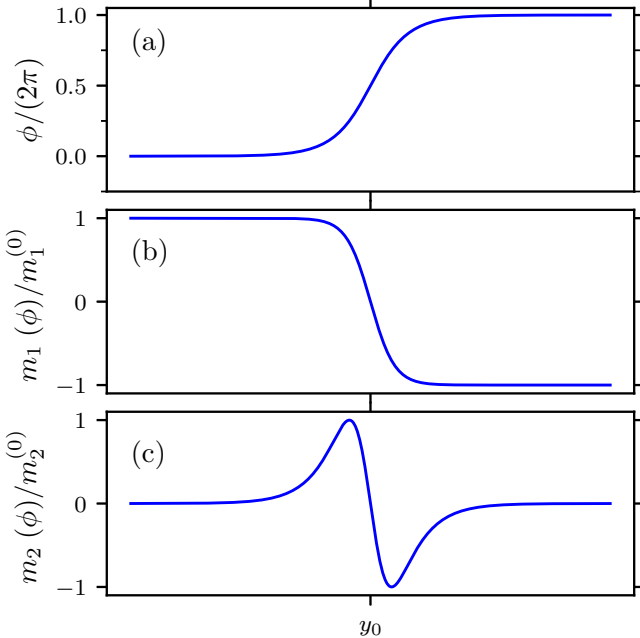


FIG. 5. Profile for a soliton of the phase (a) and the masses $m_1(\phi)$ (b) and $m_2(\phi)$ (c), respectively, for the TRITOPS-TRITOPS junction with $\phi_0 = 0.12 \times 2\pi$.

have

$$\eta(y) = (\eta_{1,\uparrow}(y), \eta_{1,\downarrow}(y), \eta_{2,\uparrow}(y), \eta_{2,\downarrow}(y))^T \quad (\text{TRITOPS-TRITOPS}). \quad (27)$$

Each of these operators is real, $\eta^\dagger(y) = \eta(y)$ as a consequence of the Majorana property $\eta_{k,j,\sigma}^\dagger = \eta_{-k,j,\sigma}$ being $\eta_{j,\sigma}(y) = \sum_k e^{-iky} \eta_{k,j,\sigma}$ [43,67]. These operators can be expressed in terms of the operators that describe the microscopic properties of the TRITOPS. For a two-dimensional system described by a Bogoliubov-de Gennes Hamiltonian in which up and down electrons form $p_x + ip_y$ and $p_x - ip_y$ pairing (see $A_{1/2u}$ and $B_{1/2u}$ representations of the pairing in Ref. [67]) they read as

$$\eta_{j,\sigma}(y) = \frac{e^{-is_j s_\sigma \pi/4}}{\sqrt{2}} (c_{j,\sigma}(y) + is_j s_\sigma c_{j,\sigma}^\dagger(y)), \quad (28)$$

where $s_j = \pm$ for the TRITOPS 1, 2, respectively, and $s_\uparrow = -s_\downarrow = 1$. Here, the operators $c_{j,\sigma}(y)$ [$c_{j,\sigma}^\dagger(y)$] destroy (create) an electron at the coordinate y along the edge in the TRITOPS j with spin σ . In the TRITOPS-S case we omit the label j .

In what follows, we analyze the existence of bound states by solving the Dirac equation

$$[m_1(y)\beta_1 + m_2(y)\beta_2 - i\hbar v \alpha \partial_y] \Psi(y) = E \Psi(y), \quad (29)$$

with the matrices α and $\beta_{1,2}$ depending on the type of junction and with the mass terms $m_{1,2}(y)$ defined by the soliton profile.

A. Single soliton

The single-soliton case defines the celebrated Jackiw-Rebbi model for a one-dimensional Dirac system with a spatially dependent mass term. This problem is known to have a zero mode localized at the point where the mass changes sign. For simplicity, we consider $y_0 = 0$ and we approximate the y dependence of the mass shown in Figs. 4 and 5 by the function $\text{sgn}(y)$. Given our results of the previous section, we consider $m_{\text{step}} = m_2$ in the case of TRITOPS-S and $m_{\text{step}} = m_1$ for the TRITOPS-TRITOPS junction, with

$$m_{\text{step}} = \pm m_0 \text{sgn}(y), \quad m_0 > 0 \quad (30)$$

for the antisoliton and soliton, respectively. For simplicity we neglect for now the smaller mass m_2 for the TRITOPS-TRITOPS junction. Below we will include this mass and avoid the approximation (30) for the shape of the mass.

The zero mode is found by solving Eq. (29) with $E = 0$. The result is

$$\Psi^{(\pm)}(y) = C \Psi_0^{(\pm)} e^{-\kappa|y|} \quad (31)$$

with C being a normalization factor, $\kappa = m_0/\hbar v$ defines the inverse of the localization length of the zero mode, and $\Psi_0^{(\pm)}$ satisfies $\alpha_0 \alpha_1 \Psi_0^{(\pm)} = \pm i \Psi_0^{(\pm)}$. The spatial dependence of the wave functions is the same for both kinds of junctions and is illustrated in Fig. 6(a). However, the structure of the spinor is different in the two types of junctions. We now show that this implies a different nature of the bound states.

For the TRITOPS-S junction there is a single solution to Eq. (29), while the TRITOPS-TRITOPS one is doubly degenerate. This reflects the fact that in the latter case time-reversal symmetry is not broken in the equilibrium phase ($\phi_{\text{eq}} = 0$), hence, there are two localized zero modes that form a Kramers

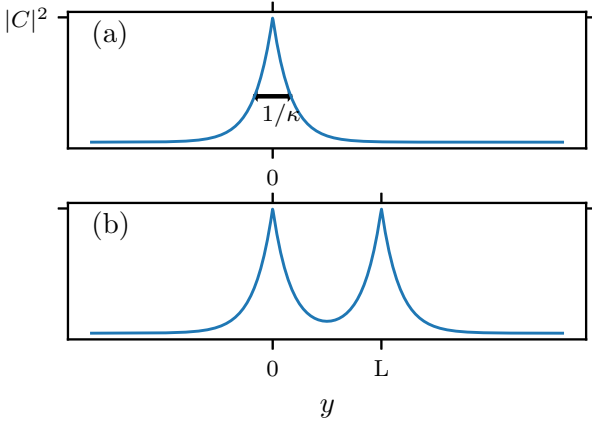


FIG. 6. (a) Probability density of the bound states of the TRITOPS-S and TRITOPS-TRITOPS junctions described by Eq. (31). (b) Probability density of the bound states of the same junctions for a soliton-antisoliton profile.

pair. In the TRITOPS-S case, time-reversal symmetry is broken ($\phi_{\text{eq}} \neq 0$), hence, it is possible to have a single solution for a given mass profile. In fact, the solution for a soliton (antisoliton) phase of type ϕ_1 is equal to the solution for an antisoliton (soliton) in the phase type ϕ_2 . The corresponding spinors are

$$\text{TRITOPS-S} \quad \Psi_0^{(\pm)} = (1, \pm 1)^T / \sqrt{2}, \quad (32)$$

$$\text{TRITOPS-TRITOPS} \quad \begin{cases} \Psi_{0,\uparrow}^{(\pm)} = (1, 0, \pm 1, 0)^T / \sqrt{2}, \\ \Psi_{0,\downarrow}^{(\pm)} = (0, 1, 0, \pm 1)^T / \sqrt{2}. \end{cases} \quad (33)$$

Taking into account Eq. (26), the resulting Bogoliubov operator in the TRITOPS-S case can be found to be

$$\begin{aligned} \text{TRITOPS-S} \quad \eta_0^{(\pm)} &= \int dy (\Psi^{(\pm)}(y))^{\dagger} \eta(y) \\ &= \frac{\tilde{\eta}_{\uparrow}(0) \pm \tilde{\eta}_{\downarrow}(0)}{\sqrt{2}}, \end{aligned} \quad (34)$$

where we have defined

$$\tilde{\eta}_{\sigma}(x) = C \int dy e^{-\kappa|y-x|} \eta_{\sigma}(y). \quad (35)$$

This zero mode η_0 is described by a Majorana operator, which can be expressed in terms of a spin- $\frac{1}{2}$ fermionic operator as follows:

$$\eta_0 = \frac{(f_0^{\dagger} + f_0)}{\sqrt{2}}, \quad f_0 = \frac{e^{i\pi/4}}{\sqrt{2}} (c_{0,\uparrow} + ic_{0,\downarrow}). \quad (36)$$

The two degenerate zero modes of the TRITOPS-TRITOPS junction have the same weight at each side of the junction and, using Eq. (27), can be combined to form the two Bogoliubov operators

$$\text{TRITOPS-TRITOPS} \quad \begin{cases} \gamma_{0,+} = \frac{\tilde{\eta}_{1,\uparrow}(0) \pm \tilde{\eta}_{2,\uparrow}(0) + i[\tilde{\eta}_{1,\downarrow}(0) \pm \tilde{\eta}_{2,\downarrow}(0)]}{2}, \\ \gamma_{0,-} = \frac{\tilde{\eta}_{1,\uparrow}(0) \pm \tilde{\eta}_{2,\uparrow}(0) - i[\tilde{\eta}_{1,\downarrow}(0) \pm \tilde{\eta}_{2,\downarrow}(0)]}{2}. \end{cases} \quad (37)$$

These operators satisfy $\gamma_{0,+} = \gamma_{0,-}^{\dagger}$, which is typical of zero modes associated to a Kramers pair of Majorana fermions [36,50,52].

Notice that these zero-energy bound states are very localized. Hence, they are not expected to play a role in the tunneling processes connecting the edge modes through the junction, which generates the effective mass $m(\phi)$ [67]. In configurations of many solitons in the junction, they could play some role and $m(\phi)$ should be calculated self-consistently.

Finally, we discuss the impact of the mass $m_2(\phi)$ on the edge-state spectrum with soliton in the TRITOPS-TRITOPS junction. As discussed, for a generic but fixed configuration this mass term breaks time-reversal symmetry. Hence, one expects the Kramers degeneracy to be lifted. However, as long as both mass terms have a well-defined parity under $y \rightarrow -y$ the spectrum continues to be doubly degenerate. For the soliton solutions discussed above, both mass terms are odd under $y \rightarrow -y$. In this case one can identify two ‘‘pseudoparity’’ operators

$$P_1 = \tilde{\sigma}^0 \sigma^x p, \quad (38)$$

$$P_2 = \tilde{\sigma}^x \sigma^z p, \quad (39)$$

with $pf(y) = f(-y)$. Both commute with the Hamiltonian \mathcal{H} of Eq. (3), but do not commute with each other. More generally, P_1 and P_2 commute with \mathcal{H} if $\phi \rightarrow 2\pi - \phi$ under $y \rightarrow -y$. Hence, the spectrum of \mathcal{H} with masses that are odd under $y \rightarrow -y$ is doubly degenerate: let Ψ_1 be a simultaneous eigenstate of \mathcal{H} and P_1 , then $\Psi_2 = P_2 \Psi_1$ is a distinct eigenstate with the same energy; the only alternative would be $\Psi_2 = 0$, which is not allowed since $P_2 \Psi_2 = \Psi_1$ due to $P_2^2 = 1$. For $m_2 = 0$ we have exactly one pair of Kramers degenerate normalizable zero modes. As charge conjugacy requires eigenstates to occur in pairs of opposite energy, the pair must remain at zero energy, i.e., the pair of zero modes cannot be split by the mass term $m_2 \beta_2$. Notice $\Psi_2 \neq \mathcal{T} \Psi_1$, i.e., the two zero modes are not Kramers pairs, but protected by the fact that both masses are odd in y . They do adiabatically connect to Kramers pairs at $m_2 \rightarrow 0$ though. In Appendix D we explicitly demonstrate the existence of doubly degenerate normalizable zero modes for given antisymmetric mass profiles $m_1(y)$ and $m_2(y)$, with $m_2(y)$ vanishing for $y \rightarrow \pm\infty$.

B. Soliton-antisoliton

Next, we analyze configurations leading to two sign changes in the mass profile. This corresponds to a soliton-antisoliton (kink-antikink) in the case of TRITOPS-TRITOPS. For the TRITOPS-S case, this can be achieved by means of a fractional soliton-antisoliton or by two fractional kinks completing the total change from 0 to 2π in the phase profile (see Fig. 4).

We consider here the following function for the mass profile, assuming abrupt changes of the mass sign at $y = 0$ and L :

$$m(y) = m_0 - 2m_0[\theta(y) - \theta(y - L)]. \quad (40)$$

The new feature in this case is the possibility of hybridization between the bound states of the single soliton when the distance between the walls is comparable with the localization length $L < 2\kappa^{-1}$. In such a scenario, we expect the energy of

these bound states to be different from zero [50,86]. Hence, we search for solutions of Eq. (29) with $E \neq 0$.

We now briefly discuss the solution of the bound states with finite energy in the case of the TRITOPS-S junction. To this end, we consider Eq. (29) with $\alpha = \sigma^z$, $\beta_2 = \sigma^y$, and $m_2(y)$ being the mass profile of Eq. (40). It is convenient to perform the rotation $U = e^{i\pi/4\sigma_y} = (\sigma_0 + i\sigma^y)/\sqrt{2}$ so that Eq. (29) is transformed to

$$[i\hbar v \partial_y \sigma^x + m(y)\sigma^y]\tilde{\Psi} = E\tilde{\Psi}, \quad (41)$$

where $\tilde{\Psi} = U\Psi = (\tilde{\psi}_1, \tilde{\psi}_2)^T$. After some algebra, we get

$$\begin{aligned} \tilde{\psi}_2 &= \frac{i}{E}[\hbar v \partial_y + m(y)]\tilde{\psi}_1, \\ [m^2(y) - \hbar^2 v^2 \partial_y^2 - \hbar v m'(y)]\tilde{\psi}_1 &= E^2 \tilde{\psi}_1. \end{aligned} \quad (42)$$

Given the profile of Eq. (40), the solutions are

$$\tilde{\psi}_1(y) = \begin{cases} -C\chi e^{\kappa(y-L)}, & y \leq 0 \\ C[-(\chi+1)e^{\kappa(y-L)} + e^{-\kappa(y+L)}], & 0 < y \leq L \\ C[-(\chi+1)e^{\kappa L} + e^{-\kappa L}]e^{-\kappa y}, & y > L \end{cases}$$

$$\tilde{\psi}_{2,\pm}(y) = \pm i\tilde{\psi}_1(-y+L), \quad (43)$$

with $\chi = \kappa \hbar v / m_0$ and

$$C = \sqrt{\frac{\kappa}{2\{\chi(\chi+1) - e^{-2\kappa L}[\chi + (\chi+1)\kappa L]\}}}. \quad (44)$$

The energies of the bound states as well as the localization length κ^{-1} of these modes are given by $E_{\pm} = \pm E(L)$ with

$$E(L) = m_0 e^{-\kappa L}, \quad \hbar^2 v^2 \kappa^2 = m_0^2 - E^2. \quad (45)$$

Notice that $|\chi| \leq 1$ and it can be verified that the solution is always normalizable. Examples of the spatial dependence of the square of the absolute value of the wave function are shown in Fig. 6(b).

The spinors in the original basis are

$$\Psi_{\pm}(y) = \frac{1}{2} \begin{pmatrix} \tilde{\psi}_1(y) \mp i\tilde{\psi}_1(-y+L) \\ \tilde{\psi}_1(y) \pm i\tilde{\psi}_1(-y+L) \end{pmatrix}. \quad (46)$$

In terms of operators these bound states can be expressed as follows:

$$\Gamma = \frac{1}{\sqrt{2}} \int dy [\tilde{\psi}_1(y)\eta_+(y) + i\tilde{\psi}_1(-y+L)\eta_-(y)], \quad (47)$$

where $\eta_{\pm}(y) = \frac{1}{\sqrt{2}}[\eta_{\uparrow}(y) \pm \eta_{\downarrow}(y)]$, while Γ^{\dagger}, Γ is a Bogoliubov operator that creates or annihilates a fermionic excitation with energy E_{\pm} given by Eq. (45).

The TRITOPS-TRITOPS case is similar, but with two degenerate states corresponding to combinations of the zero modes localized at $y=0, L$, with the energy given by Eq. (45). These degenerate bound states for positive energy can be described with the following Bogoliubov operators:

$$\Gamma_{\uparrow,+} = \frac{1}{\sqrt{2}} \int dy [\tilde{\psi}_1(y)\eta_{\uparrow,+}(y) + i\tilde{\psi}_1(-y+L)\eta_{\uparrow,-}(y)], \quad (48)$$

$$\Gamma_{\downarrow,+} = \frac{1}{\sqrt{2}} \int dy [\tilde{\psi}_1(y)\eta_{\downarrow,+}(y) + i\tilde{\psi}_1(-y+L)\eta_{\downarrow,-}(y)], \quad (49)$$

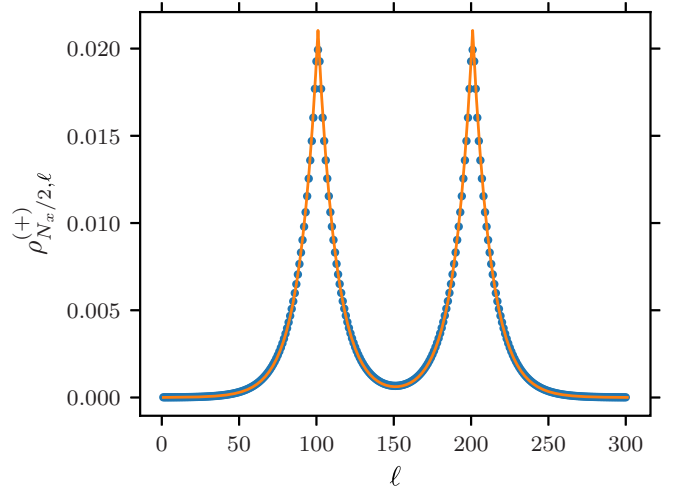


FIG. 7. Local particle density $\rho_{N_x/2,\ell}^{+}$ plotted against the sites of the topological edge of the junction calculated with respect to an E_{+} localized mode for a kink-antikink profile ϕ_{ℓ} in a S_1 - $S_2 \equiv$ TRITOPS-S junction with $\phi_0 = 0.12 \times \pi$. Parameters are $\mu = -2w$, $t_J = \Delta_p^{(1)} = \Delta_s^{(2)} = 4\Delta_s^{(1)} = w/5$, $N_1 = 100$, $N_2 = 200$, and $N_x = N_y = 300$. The line corresponds to Eq. (46) with $m_0 = 0.0037$ and $v = 0.088$.

where $\eta_{\sigma,\pm}(y) = \frac{1}{\sqrt{2}}[\eta_{\sigma,\uparrow}(y) \pm \eta_{\sigma,\downarrow}(y)]$, while those corresponding to the negative-energy states are described with

$$\Gamma_{\sigma,-} = \Gamma_{\bar{\sigma},+}^{\dagger}, \quad \sigma = \uparrow, \downarrow, \quad (50)$$

with $\bar{\uparrow} = \downarrow$ and $\bar{\downarrow} = \uparrow$.

C. Numerical benchmark

We now compare the solutions obtained on the basis of the effective Hamiltonian with numerical results calculated with the Hamiltonians described in Appendix A, which are defined in finite lattices with $N_x = 300$ sites in the x direction and $N_y = 300$ sites along the junction. In the present case we consider open boundary conditions along both directions.

We diagonalize the Hamiltonian in Eq. (A1) and calculate the local particle density at the topological side of the TRITOPS-S junction corresponding to the two states $|\pm\rangle$, which are identified as those associated to the bound states at the kink and antikink, with energy E_{\pm} ,

$$\rho_{N_x,\ell}^{\pm} = \sum_{\sigma=\uparrow,\downarrow} \langle \pm | c_{N_x,\ell,\sigma}^{\dagger} c_{N_x,\ell,\sigma} | \pm \rangle = \frac{1}{2} \langle s | \mathbf{c}_{N_x,\ell}^{\dagger} \boldsymbol{\tau}^z \mathbf{c}_{N_x,\ell} | s \rangle, \quad (51)$$

being $\mathbf{c}_{N_x,\ell} = (c_{N_x,\ell,\uparrow}, c_{N_x,\ell,\downarrow}, c_{N_x,\ell,\uparrow}^{\dagger}, -c_{N_x,\ell,\downarrow}^{\dagger})^T$.

Results for the local particle density $\rho_{\ell,N_x}^{(+)}$ illustrating the case of a kink-antikink profile in a TRITOPS-S junction are shown in Fig. 7. These are calculated with the following profile for the phase bias:

$$\phi_{\ell} = \begin{cases} \phi_0, & \ell = 1, \dots, N_1 - 1, N_2 + 1, \dots, N_y \\ \pi, & \ell = N_1, \ell = N_2 \\ 2\pi - \phi_0, & \ell = N_1, \dots, N_2 \end{cases} \quad (52)$$

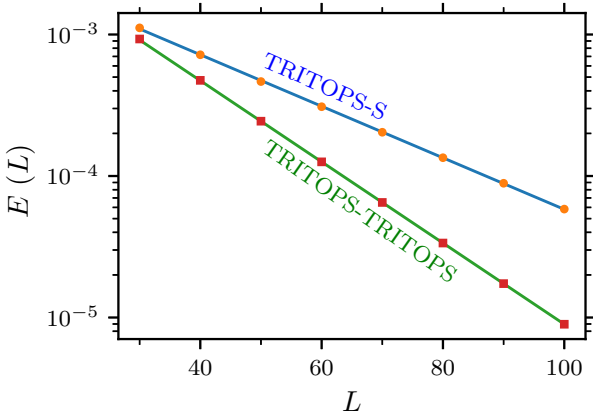


FIG. 8. TRITOPS-S: energy due to the hybridization between solitons as function of the distance L between solitons with $\mu = -2w$, $t_J = \Delta_p^{(1)} = \Delta_s^{(2)} = 4\Delta_s^{(1)} = t/5$, and $N_x = N_y = 300$. TRITOPS-TRITOPS: same with $\mu = -2w$, $5t_J = \Delta_p^{(1)} = t/5$, $N_x = 150$, $N_y = 300$. Assuming $\kappa \approx m_0/\hbar v$, the linear fit corresponds to $\log(E) = -\frac{m_0}{\hbar v}L + \log(m_0)$ obtaining $m_0 = 0.0037$ and $\hbar v = 0.088$ for the TRITOPS-S case and $m_0 = 0.0067$ and $\hbar v = 0.102$ for TRITOPS-TRITOPS.

where N_1 and N_2 are the positions of the kink and antikink, respectively. The results of Fig. 7 correspond to $\phi_0 = 0.12 \times \pi$. The energy of this bound state is very small ($\sim 10^{-4}$), in consistency with the limit $L = N_2 - N_1 = 100 \gg 1$ of Eq. (45). In the figure we also show a fit with a function of the form given by Eq. (46), indicating the considered values of m_0 and v , while κ has been calculated by solving Eq. (45).

As the distance between solitons gets shorter, the energy increases exponentially following Eq. (45). This behavior is illustrated in Fig. 8 for the two types of junctions and considering the profile of Eq. (52) with $\phi_0 = 0.12 \times \pi$ in the case of the TRITOPS-S junction and $\phi_0 = 0$ for the TRITOPS-TRITOPS one. Assuming that the separation between kink and antikink is still large, one can approximate $\kappa \approx m_0/v$ in Eq. (45). From there we can get an estimation of the mass m_0 and the velocity v as indicated in the caption of Fig. 8. We recall that the relation between the parameters of the effective continuum model and the lattice Hamiltonian is as follows: $m_0 < |t_J|^2/\Delta_{\text{eff}}$ for the TRITOPS-S junction and $m_0 < |t_J|$ for the TRITOPS-TRITOPS one, while the velocity of the edge modes is $v < \Delta_{\text{eff}}$ [67]. Therefore, we find a perfect consistency between the description of the bound states in terms of the effective continuum model introduced in Sec. V and the exact numerical results.

VI. DYNAMICS OF THE SOLITON-ANTISOLITON WITH THE BOUND STATES

In the previous sections, the focus was on the description of the static problem of the phase bias along the junction defined by the effect of the CPR, as well as the description of the electron bound states enabled by the phase profile. The aim of this section is to discuss the expected dynamics for the coupled system.

The problem of kink-antikink collisions vs the formation of an oscillating breather bound state in the context of the usual

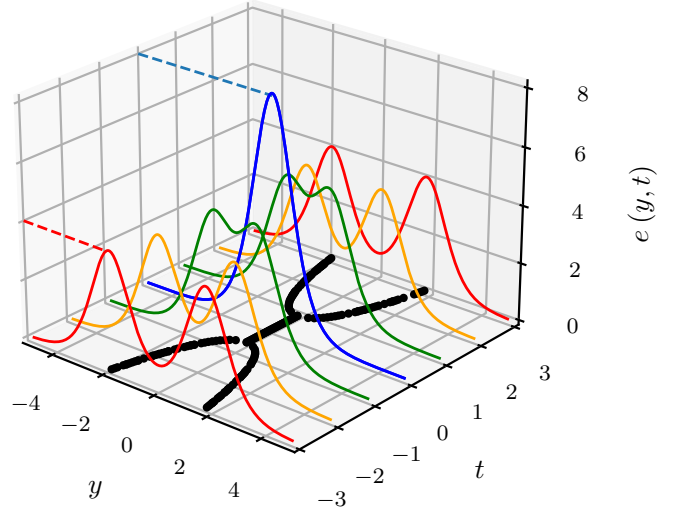


FIG. 9. Energy density for a collision between a kink and an antikink pair with initial velocity $V_k = 0.1$ with $\kappa = m_0/\hbar v = 1$. Black lines correspond to soliton trajectories corresponding to the maximum of the energy density at each given time. Notice that energy is conserved.

sine-Gordon equation has a long story [76]. The different scenarios can be analyzed by investigating the time-dependent energy density of the Hamiltonian leading to Eq. (14),

$$H_\phi = \int dy \left[\frac{1}{2} \phi_t^2 + \frac{1}{2} \phi_y^2 + \epsilon(\phi) \right], \quad (53)$$

with

$$\epsilon(\phi) \equiv \epsilon_{\text{SG}} = 1 - \cos(\phi). \quad (54)$$

This equation is valid for the TRITOPS-TRITOPS junction. For the integrable case of the TRITOPS-S junction, we have Eq. (20) instead of Eq. (54). In what follows we focus on the TRITOPS-TRITOPS case, and we rely on known analytical results of the dynamics of the usual sine-Gordon model [69]. The conclusions will be similar for the other junction.

In the framework of the usual sine-Gordon Hamiltonian, kink and antikink solutions traveling in opposite directions with initial velocities $\pm V_k$ are described by the following expression:

$$\phi_{\text{SG}}(y, t) = 4 \arctan \left[\frac{V_k \cosh(\delta_k y)}{\sinh(\delta_k V_k t)} \right], \quad (55)$$

with $\delta_k = 1/\sqrt{1 - V_k^2}$. The energy density corresponding to the traveling solitons without taking into account the fermionic states is

$$e(y, t) = \frac{1}{2} \phi_t^2 + \frac{1}{2} \phi_y^2 + \epsilon(\phi). \quad (56)$$

The behavior of this function is illustrated in Fig. 9 for a given value of the initial velocity. The total energy is conserved. In particular, we see that by adding the maxima of $e(y, t)$ for the two separate solitons we get the maximum at the collision, reflecting the fact that the collision is perfectly elastic. The trajectory defined by these maxima as functions of time is plotted in the horizontal plane. The kink and antikink preserve their shape thereafter and, as they approach, they accelerate.

The result is a shift in the trajectories of each soliton with respect to the trajectory without collision [76].

The aim of the present section is to discuss the behavior of the joint time-dependent energy density corresponding to the Hamiltonian (53) for the phase as well the time-dependent energy of the bound states. We consider the case of a slow motion of the phase profile, so that we can describe the dynamics of the hybridized fermionic modes as a sequence of snapshots where the states have energy $E[L(t)]$ given by Eq. (45).

When the soliton and antisoliton are far apart, the electron states have zero energy, hence, we expect that their propagation takes place following the description of Eq. (56). However, as they approach, the bound states hybridize. We calculate $L(t)$ from the distance between the maxima of the energy density as a function of time predicted by Eq. (56). This approach is valid as long the soliton shape is well defined (before and after the collision). For sufficiently large L , we can approximate Eq. (45) by $E_{\pm}(L) \approx \pm m_0 e^{-\frac{m_0}{\hbar v} L}$. In this regime, we express the Hamiltonian for the subgap fermionic modes as follows:

$$H_f(L) = \frac{1}{2} \sum_{s=\pm} \sum_{\sigma=\uparrow,\downarrow} E_s(L) \Gamma_{\sigma,s}^{\dagger} \Gamma_{\sigma,s}, \quad (57)$$

with $\Gamma_{\sigma,s}$, $\sigma = \uparrow, \downarrow$, $s = \pm$ given by Eq. (49). Using the relations obeyed by the operators describing the positive- and negative-energy states, Eq. (50), we can also express this Hamiltonian as follows:

$$H_f(L) = E_+(L) \sum_{\sigma} \Gamma_{\sigma,+}^{\dagger} \Gamma_{\sigma,+} - E_+(L). \quad (58)$$

The extra contribution to the total energy originated in the subgap fermionic states depends on the nature and the evolution of the many-body state. If the zero modes of the large- L configuration are occupied by two fermions, the traveling kink and antikink experience an effective attraction of amplitude $-E_+(L)$ as L overcomes the critical length $\xi_c \simeq \hbar v/m_0$. Instead, if the zero modes are occupied by four fermions in the separated solitons, they experience a repulsion of amplitude $E_+(L)$ as they approach. Furthermore, it is possible to have a change in the parity of the ground state because of excitations of single quasiparticles near defects. In such a case, it is also possible to have a single occupied state with positive energy, and the fermionic states are neutral regarding the soliton dynamics. The behavior of $E_+[L(t)]$ as a function of time is shown in Fig. 10. Interestingly, a very similar discussion was earlier presented in the context of fermionic energies in a multisoliton background [87].

In the case of the TRITOPS-S junction, we can follow a similar reasoning by assuming that the soliton-antisoliton dynamics is also described by Eq. (55) and by the following Hamiltonian:

$$H_f(L) = E_+(L) \Gamma_{+}^{\dagger} \Gamma_{+} - E_+(L)/2. \quad (59)$$

In this junction, the two Majorana fermions localized at the kink and at the antikink combine in a fermionic mode as they approach one another. This results in an attraction equal to $-E_+(L)/2$. In the presence of poisoning corresponding to a change in the parity of the many-body ground state, the positive-energy state is occupied, which generates a repulsion of amplitude $E_+(L)/2$.

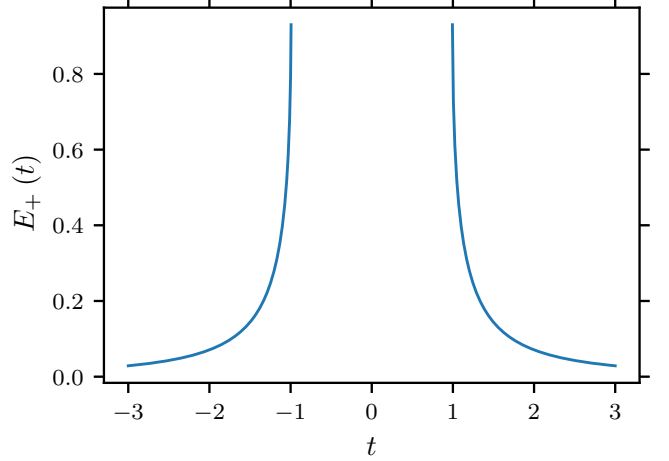


FIG. 10. Energy as a function of the distance of the fermionic bound-state repulsion, being $\kappa = m_0/\hbar v = 1$.

VII. SUMMARY AND CONCLUSIONS

We have analyzed the joint dynamics of the phase bias ϕ and the Majorana edge modes at the different types of Josephson junctions formed with two-dimensional (2D) time-reversal invariant topological superconductors (TRITOPS). In particular, we have considered TRITOPS-TRITOPS and junctions between a TRITOPS and a nontopological superconductor (TRITOPS-S). The analysis is mainly based on effective models for the junctions, which consist of Dirac Hamiltonians with mass depending on the phase bias and the results are contrasted against the numerical solutions of lattice models. We have extended the study of Ref. [77], which focused on junctions of 2D topological superconductors with broken time-reversal symmetry (class D) in two main directions. In the case of the TRITOPS-TRITOPS junction we have considered both the direct hybridization between the topological edge modes and the hybridization between these modes, and the supragap states of the superconductor at the other side of the junction. The latter is a second-order process that generates an extra effective mass, which couples the two partners of the edge Kramers' pair of each TRITOPS. In the case of the TRITOPS-S junctions this is the only massive term playing a role.

We have first analyzed the effect of the phase fluctuations. These may play a critical role in the case of TRITOPS-S junctions and may destroy the stability of a state with broken time-reversal symmetry. We have shown that the phase stiffness must overcome a critical value for the mean-field description to be stable.

As a second step, assuming the stability of the mean-field description for the phase, we have analyzed the effect of fluxons in the junction. This defines a sine-Gordon model (for the TRITOPS-TRITOPS) and a double sine-Gordon model (for the TRITOPS-S case). We have calculated the solitonic profiles of the kink and antikink solutions of these models. These generate changes in the sign of the mass term of the Dirac Hamiltonians describing the coupling of the Majorana edge states.

Therefore, the third step was to study the impact of the solitonic profiles on the fermionic states. We have shown the existence of zero modes localized at the fluxons. These are Majorana zero modes in the case of a TRITOPS-S junction and a Kramers pair of Majorana modes in the case of the TRITOPS-TRITOPS junction. In the latter case, we have shown that these zero modes remain robust against the effect of the second-order mass term, in spite of the fact that this term breaks time-reversal symmetry. This property is due to extra symmetries of the junction, assuming spin-preserving tunneling processes. The existence of such localized zero modes is very interesting in view of potential applications since they can be manipulated and moved in these systems by the motions of the fluxons at the junction.

Finally, we have analyzed the effect of the localized fermionic modes in the collision dynamics of solitons and antisolitons. While such a collision is perfectly elastic in nontopological junctions, the hybridized zero modes of the junctions studied in this paper originate an effective attractive or repulsive interaction, depending on the occupation of these modes. These properties should be very useful for the experimental detection of these states.

ACKNOWLEDGMENTS

We are grateful to A. Ustinov for many interesting discussions. A.S. is also grateful to J. D. Sau and V. Yakovenko for illuminating discussions. L.A. and G.R.R. thank support from CONICET as well as FonCyT, Argentina, through Grants No. PICT-2018-04536 and No. PICT 2020-A-03661. We also thank support from Alexander von Humboldt foundation (L.A.) and the SPUK collaboration (J.S. and L.A.). A.R. and A.S. were supported by the DFG under the Grant No. SH81/7-1. J.S. was supported by DFG through Project No. ER 463/14-1 and acknowledges a Weston Visiting Professorship at the Weizmann Institute of Science where part of this work was performed. L.A. would also like to thank the Institut Henri Poincaré (UAR 839 CNRS-Sorbonne Université) and the LabEx CARMIN (ANR-10-LABX-59-01) for their support.

APPENDIX A: LATTICE MODEL FOR THE JUNCTION

We consider the Hamiltonian

$$H = \sum_{\ell=1}^{N_y} H_{\ell}, \quad H_{\ell} = \sum_{\alpha=S_1, S_2} H_{\alpha, \ell} + H_{J, \ell}. \quad (A1)$$

The Hamiltonian $H_{\alpha, \ell}$ corresponds to the TRITOPS Hamiltonian expressed in a ribbon with N_y sites along the junction and N_x sites in the other direction. The Hamiltonian for the tunneling junction is $H_J = \sum_{\ell} H_{J, \ell}$, with

$$H_{J, \ell} = t_J \sum_{\sigma} (e^{i\phi_{\ell}/2} c_{\ell, 1\sigma}^{\dagger} c_{\ell, 2\sigma} + \text{H.c.}), \quad (A2)$$

where $c_{\ell, 1\sigma}^{\dagger}$ ($c_{\ell, 2\sigma}^{\dagger}$) creates an electron with spin σ in the superconductor S1 (S2) at the site located at the boundary contacting the junction. The phase bias at the junction contains the information of the soliton profile.

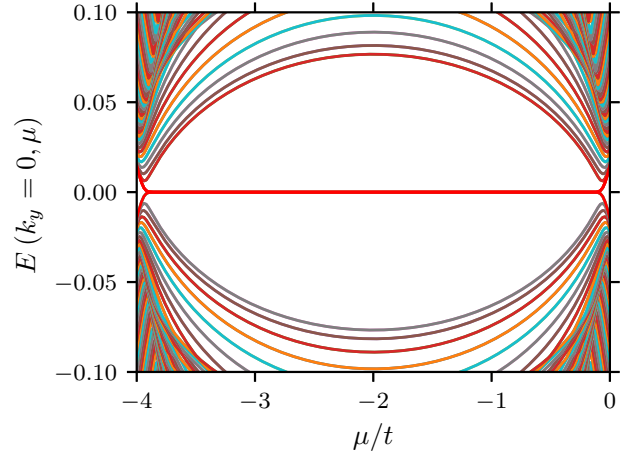


FIG. 11. Energy for the states with $k_y = 0$ vs μ for a TRITOPS superconductor periodic in the y direction with $\Delta_p = 4\Delta_s = w/5$ and $w = 1$. The topological phase corresponds to the values of μ with double-degenerate zero-energy states (depicted in red).

The Hamiltonian for the TRITOPS formulated in the reciprocal space reads as $H = \frac{1}{2} \sum_{\mathbf{k}} \mathbf{c}_{\mathbf{k}}^{\dagger} H_{\mathbf{k}} \mathbf{c}_{\mathbf{k}}$, with $\mathbf{c}_{\mathbf{k}} = (c_{\mathbf{k}, \uparrow}, c_{\mathbf{k}, \downarrow}, c_{-\mathbf{k}, \downarrow}^{\dagger}, -c_{-\mathbf{k}, \uparrow}^{\dagger})^T$ and $\mathbf{k} = (k_x, k_y)$, while the Bogoliubov-de Gennes Hamiltonian matrix reads as

$$H_{\mathbf{k}} = \xi_{\mathbf{k}} \tau^z S^0 + \tau^x \mathbf{S} \cdot \Delta_{\mathbf{k}}^{x,y} + \tau^x S^0 \Delta_s. \quad (A3)$$

The Pauli matrices $\tau^{x,y,z}$ and $\mathbf{S} = (S^x, S^y, S^z)$ act, respectively, on the particle hole and spin degrees of freedom, while τ^0, S^0 are 2×2 identity matrices. The dispersion relation is defined in terms of a hopping element w as $\varepsilon_{\mathbf{k}} = -2w(\cos k_x + \cos k_y)$, hence $\xi_{\mathbf{k}} = \varepsilon_{\mathbf{k}} - \mu$, being μ the chemical potential. For simplicity, we consider only nearest-neighbor hopping in $\varepsilon_{\mathbf{k}}$. For the TRITOPS we consider a p -wave pairing term defined by

$$\Delta_{\mathbf{k}}^{x,y} = \Delta_p (\sin k_x \mathbf{n}^x + \sin k_y \mathbf{n}^y), \quad (A4)$$

with $\mathbf{n}^{x,y}$ being unit vectors along the x, y directions along with a local s -wave component modulated by Δ_s . We choose the values of the parameters corresponding to the topological phase. To verify this property we confirm the existence of Kramers pairs of topological edge states as shown in Figs. 11 and 12. The nontopological superconductor (S) is modeled with $\Delta_p = 0$, $\Delta_s \neq 0$.

APPENDIX B: SYMMETRIES OF THE TRITOPS-TRITOPS JUNCTION

Consider the continuum limit of the Hamiltonian in (A3), modeling a TRITOPS with p -wave pairing, which up to leading order in the momenta and with $\Delta_s = 0$ reads as

$$\mathcal{H}^{(\pm)} = -\mu^{(\pm)}(x) \tau^z S^0 + v \tau^x (p_x S^x + p_y S^y). \quad (B1)$$

$\mu(x)$ is assumed to change sign at the edge of a given sample and the topological phase corresponds to $\mu/v > 0$. Thus, we distinguish $\mu^{(+)}(x \gtrless 0) \lesseqgtr 0$ and $\mu^{(-)}(x \gtrless 0) \gtrless 0$ describing right and left edges, respectively. For $p_y = 0$, we find in each case two normalizable zero modes bound to the respective

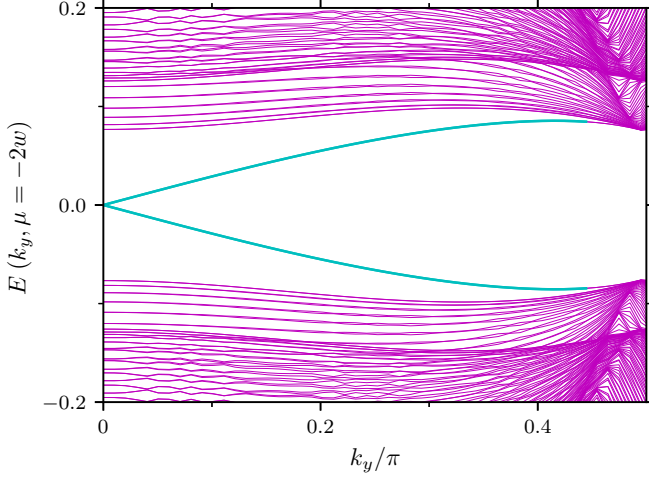


FIG. 12. Energy for the states with $\mu = -2w$ vs k_y for a TRI-TOPS superconductor periodic in the y direction with $\Delta_p = 4\Delta_s = w/5$ and $w = 1$. The topological edge states correspond to the double-degenerate states inside the gap (depicted in light blue).

edge satisfying $\mathcal{H}\Phi_0(x) = 0$ given by

$$\begin{aligned}\Phi_{0,\uparrow}^{(\pm)}(x) &= \frac{N}{2} e^{\pm \int_0^x dx' \mu(x')/v} (1 \pm i, 0, 0, -1 \pm i)^T, \\ \Phi_{0,\downarrow}^{(\pm)}(x) &= \frac{N}{2} e^{\pm \int_0^x dx' \mu(x')/v} (0, 1 \mp i, 1 \pm i, 0)^T.\end{aligned}\quad (\text{B2})$$

Note that the solutions are chosen such that they are orthonormal and are invariant under charge conjugation $C\Phi_{0,\sigma}^{(\pm)}(0) = \Phi_{0,\sigma}^{(\pm)}(0)$, where the charge-conjugation operator is given by $C = \tau^y S^y \mathcal{K} \equiv \mathcal{U}_C \mathcal{K}$. Additionally, it is worth noting that the two respective solutions are Kramer's pairs $\mathcal{T}\Phi_{0,\downarrow}^{(\pm)} = \Phi_{0,\uparrow}^{(\pm)}$, with the time-reversal operator $\mathcal{T} = iS^y \mathcal{K}$. Including finite momenta p_y entails projecting the corresponding term in the Hamiltonian onto this basis, which yields

$$(\Phi_{0,\sigma}^{(\tau)}(0))^\dagger \tau^x S^y \Phi_{0,\sigma'}^{(\tau')}(0) = (\tilde{\sigma}^z)^{\tau,\tau'} (\sigma^z)^{\sigma,\sigma'}, \quad (\text{B3})$$

as given in Eq. (6). Transforming the antiunitary operators C and \mathcal{T} to this basis, one finds $C = \mathcal{K}$ and $\mathcal{T} = i\sigma^y \mathcal{K}$.

Additionally, we can identify the symmetry corresponding to exchanging the right and the left edge with each other. On the level of the Hamiltonian in (B1), this is achieved by simultaneous inversion along the x axis P_x , i.e., $P_x f(x) = f(-x)$, and rotating with $U_X = \tau^z S^x$:

$$(U_X P_x) \mathcal{H}^{(\pm)} (P_x U_X) = -\mu^{(\pm)}(-x) \tau^z + v \tau^x (p_x S^x + p_y S^y). \quad (\text{B4})$$

This is the same Hamiltonian as (B1) only with the direction of the sign change of μ , which determined whether we called it a right or left edge, reversed. U_X connects the right and left edge modes in (B2) with each other

$$U_X \Phi_{0,\uparrow}^{(+)} = \Phi_{0,\downarrow}^{(-)}, \quad U_X \Phi_{0,\uparrow}^{(-)} = \Phi_{0,\downarrow}^{(+)}. \quad (\text{B5})$$

Expressed in the new basis, it therefore holds

$$U_X = \tilde{\sigma}^x \sigma^x. \quad (\text{B6})$$

APPENDIX C: DERIVATION OF THE FLUCTUATION-CORRECTED EQUATION OF STATE

In order to derive the fluctuation-corrected equation of state in (11), following Ref. [68], we expand the action in Eq. (10) up to second order in the fluctuations $\delta\phi$ around some assumed minimum $\langle\phi\rangle = \tilde{\phi}$ of the ground-state energy $\phi(x, t) = \tilde{\phi} + \delta\phi(x, t)$. After a Wick rotation to Euclidean time and integrating out the fermions, we find the effective action at some temperature T and length of the system L to read as

$$\begin{aligned}S_{\text{eff}} &= \frac{1}{2} \frac{T}{L} \sum_{q, \omega_m} \mathcal{D}^{-1}(q, \omega_m) |\delta\phi(q, \omega_m)|^2 \\ &\quad + \frac{1}{2} \frac{L}{T} E_J \tilde{\phi}^2 - \frac{1}{2} \text{tr} \log \mathcal{G}_0^{-1},\end{aligned}\quad (\text{C1})$$

where

$$\mathcal{D}^{-1}(q, \omega_m) = \hbar K \left(\frac{\omega_m^2}{c_J} + c_J q^2 \right) + E_J + \Pi(q, \omega_m), \quad (\text{C2})$$

with

$$\begin{aligned}\Pi(q, \omega_m) &= \frac{m_0^2}{4} \frac{T}{L} \sum_{k, \epsilon_n} \text{tr}_{2 \times 2} [\mathcal{G}_0(k, \epsilon_n) \alpha_0 \\ &\quad \times \mathcal{G}_0(k + q, \epsilon_n + \omega_m) \alpha_0]\end{aligned}\quad (\text{C3})$$

and

$$\mathcal{G}_0^{-1} = \begin{pmatrix} \hbar(\partial_\tau - iv\partial_y) & -im_0\tilde{\phi} \\ im_0\tilde{\phi} & \hbar(\partial_\tau + iv\partial_y) \end{pmatrix}. \quad (\text{C4})$$

ω_m and ϵ_n are the bosonic and fermionic Matsubara frequencies, respectively. The ground-state energy density in terms of $\tilde{\phi}$ can now be determined from $E(\tilde{\phi}) = (-\frac{T}{L} \log \int \mathcal{D}(\delta\phi) e^{-S_{\text{eff}}})_{T \rightarrow 0}$. Differentiating this expression with respect to $\tilde{\phi}^2$ finally results in Eq. (11) of the main text, where we used [88] that for $T \rightarrow 0$

$$\Pi(q, \omega) = \frac{m_0^2}{4\pi\hbar v} \left[\frac{1}{2} \log \left(\frac{m_0^2 \tilde{\phi}^2}{4\Lambda^2} \right) + \frac{\sqrt{1+r^2}}{r} \text{Arsinh}(r) \right] \quad (\text{C5})$$

with $r = \hbar\sqrt{\omega^2 + v^2 q^2} / (2m_0\tilde{\phi})$.

APPENDIX D: ZERO-ENERGY SOLUTIONS TO DOUBLE MASS DIRAC EQUATION

The Dirac equation for zero modes in the TRITOPS-TRITOPS junction in the presence of a phase slip soliton reads as

$$(-i\hbar v \partial_y \tilde{\sigma}^z \sigma^z + m_1(y) \tilde{\sigma}^y \sigma^z + m_2(y) \tilde{\sigma}^0 \sigma^y) \psi(y) = 0 \quad (\text{D1})$$

$$\Leftrightarrow (\hbar v \partial_y + m_1(y) \tilde{\sigma}^x \sigma^0 + m_2(y) \tilde{\sigma}^z \sigma^x) \psi(y) = 0, \quad (\text{D2})$$

where asymptotically $m_1(y \rightarrow \pm\infty) = \pm m_1^{(0)}$ and $m_2(y \rightarrow \pm\infty) = 0$ with both mass terms antisymmetric $m_{1,2}(y) = -m_{1,2}(-y)$. Note that $m_2 \neq 0$ breaks time-reversal symmetry and one would thus expect the Kramer's degeneracy to be lifted in its presence. However, as argued in the main text, this turns out not to be the case if both masses have well-defined

parity, due to the existence of the two noncommuting “pseudoparities” $P_1 = \tilde{\sigma}^0 \sigma^x p$ and $P_2 = \tilde{\sigma}^x \sigma^z p$ (see the discussion in Sec. V A). As a consequence, the twofold degeneracy of the zero modes bound to the soliton also persists. Here, in order to demonstrate this, we will explicitly derive the two zero-mode solutions to Eq. (D2) in the simple case of the soliton profile being given by

$$m_1(y) = m_1^{(0)} \text{sgn}(y), \quad (\text{D3})$$

$$m_2(y) = m_2^{(0)} \text{sgn}(y) \Theta(W/2 - |y|). \quad (\text{D4})$$

We start by looking for a solution $|\psi_1\rangle$ to (D2) which is simultaneously an eigenvector of P_1 and make the ansatz

$$|\psi_1\rangle = |\xi_1\rangle \otimes |+\rangle, \quad (\text{D5})$$

where $\sigma_x |\pm\rangle = \pm |\pm\rangle$. Equation (D2) then reduces to

$$(i\hbar v \partial_y + m_1(y) \tilde{\sigma}_x + m_2(y) \tilde{\sigma}_z) \xi_1 = 0, \quad (\text{D6})$$

to which the normalizable solution can be found to read as

$$\xi_1(y) \propto \begin{cases} \begin{pmatrix} 1 \\ 1 \end{pmatrix} e^{m_1^{(0)}(y+W/2)}, & y < -W/2 \\ \begin{pmatrix} 1 \\ 1 \end{pmatrix} \cosh\left(\frac{y+W/2}{\lambda}\right) + \lambda \begin{pmatrix} m_1^{(0)} + m_2^{(0)} \\ m_1^{(0)} - m_2^{(0)} \end{pmatrix} \sinh\left(\frac{y+W/2}{\lambda}\right), & -W/2 < y < 0 \\ \begin{pmatrix} 1 \\ 1 \end{pmatrix} \cosh\left(\frac{y-W/2}{\lambda}\right) - \lambda \begin{pmatrix} m_1^{(0)} + m_2^{(0)} \\ m_1^{(0)} - m_2^{(0)} \end{pmatrix} \sinh\left(\frac{y-W/2}{\lambda}\right), & 0 < y < W/2 \\ \begin{pmatrix} 1 \\ 1 \end{pmatrix} e^{-m_1^{(0)}(y-W/2)}, & y > W/2 \end{cases} \quad (\text{D7})$$

where we introduced $(m_1^{(0)})^2 + (m_2^{(0)})^2 \equiv \lambda^{-2}$. The second, degenerate zero mode $|\psi_2\rangle$ is then found by application of P_2 to the first solution

$$|\psi_2\rangle = P_2 |\psi_1\rangle = \tilde{\sigma}^x |\xi_1\rangle \otimes |-\rangle. \quad (\text{D8})$$

Note that for $m_2^{(0)} \rightarrow 0$, $|\psi_1\rangle$ and $|\psi_2\rangle$ are indeed transformed into one another by the time-reversal operator \mathcal{T} .

It is easy to check that for mass profiles of the form as given in (D3) and (D4), but with an added asymmetry of some

sort, in general no nontrivial solutions to Eq. (D2) and thus no zero modes exist. Their degeneracy and thus existence are dependent on the parity and with that also sensitive to any impurities or inhomogeneities.

-
- [1] B. A. Bernevig, *Topological Insulators and Topological Superconductors* (Princeton University Press, Princeton, NJ, 2013).
 - [2] X.-G. Wen, Colloquium: Zoo of quantum-topological phases of matter, *Rev. Mod. Phys.* **89**, 041004 (2017).
 - [3] A. Y. Kitaev, Fault-tolerant quantum computation by anyons, *Ann. Phys.* **303**, 2 (2003).
 - [4] C. Nayak, S. H. Simon, A. Stern, M. Freedman, and S. D. Sarma, Non-Abelian anyons and topological quantum computation, *Rev. Mod. Phys.* **80**, 1083 (2008).
 - [5] S. M. Albrecht, A. P. Higginbotham, M. Madsen, F. Kuemmeth, T. S. Jespersen, J. Nygård, P. Krogstrup, and C. Marcus, Exponential protection of zero modes in majorana islands, *Nature (London)* **531**, 206 (2016).
 - [6] A. Das, Y. Ronen, Y. Most, Y. Oreg, M. Heiblum, and H. Shtrikman, Zero-bias peaks and splitting in an Al-InAs nanowire topological superconductor as a signature of majorana fermions, *Nat. Phys.* **8**, 887 (2012).
 - [7] S. Deng, L. Viola, and G. Ortiz, Majorana modes in time-reversal invariant s-wave topological superconductors, *Phys. Rev. Lett.* **108**, 036803 (2012).
 - [8] R. M. Lutchyn, J. D. Sau, and S. Das Sarma, Majorana fermions and a topological phase transition in semiconductor-superconductor heterostructures, *Phys. Rev. Lett.* **105**, 077001 (2010).
 - [9] V. Mourik, K. Zuo, S. M. Frolov, S. Plissard, E. P. Bakkers, and L. P. Kouwenhoven, Signatures of majorana fermions in hybrid superconductor-semiconductor nanowire devices, *Science* **336**, 1003 (2012).
 - [10] Y. Oreg, G. Refael, and F. Von Oppen, Helical liquids and majorana bound states in quantum wires, *Phys. Rev. Lett.* **105**, 177002 (2010).
 - [11] L. P. Rokhinson, X. Liu, and J. K. Furdyna, The fractional ac josephson effect in a semiconductor-superconductor nanowire as a signature of majorana particles, *Nat. Phys.* **8**, 795 (2012).
 - [12] H. Kim, A. Palacio-Morales, T. Posske, L. Rózsa, K. Palotás, L. Szunyogh, M. Thorwart, and R. Wiesendanger, Toward tailoring majorana bound states in artificially constructed magnetic atom chains on elemental superconductors, *Sci. Adv.* **4**, eaar5251 (2018).
 - [13] S. Nadj-Perge, I. K. Drozdov, J. Li, H. Chen, S. Jeon, J. Seo, A. H. MacDonald, B. A. Bernevig, and A. Yazdani, Observation of majorana fermions in ferromagnetic atomic chains on a superconductor, *Science* **346**, 602 (2014).
 - [14] M. Ruby, F. Pientka, Y. Peng, F. Von Oppen, B. W. Heinrich, and K. J. Franke, End states and subgap structure in proximity-coupled chains of magnetic adatoms, *Phys. Rev. Lett.* **115**, 197204 (2015).

- [15] L. Fu and C. L. Kane, Josephson current and noise at a superconductor/quantum-spin-Hall-insulator/superconductor junction, *Phys. Rev. B* **79**, 161408 (2009).
- [16] A. Fornieri, A. M. Whiticar, F. Setiawan, E. Portolés, A. C. Drachmann, A. Keselman, S. Gronin, C. Thomas, T. Wang, R. Kallaher *et al.*, Evidence of topological superconductivity in planar Josephson junctions, *Nature (London)* **569**, 89 (2019).
- [17] A. Haim and A. Stern, Benefits of weak disorder in one-dimensional topological superconductors, *Phys. Rev. Lett.* **122**, 126801 (2019).
- [18] S. Hart, H. Ren, M. Kosowsky, G. Ben-Shach, P. Leubner, C. Brüne, H. Buhmann, L. W. Molenkamp, B. I. Halperin, and A. Yacoby, Controlled finite momentum pairing and spatially varying order parameter in proximitized HgTe quantum wells, *Nat. Phys.* **13**, 87 (2017).
- [19] F. Pientka, A. Keselman, E. Berg, A. Yacoby, A. Stern, and B. I. Halperin, Topological superconductivity in a planar josephson junction, *Phys. Rev. X* **7**, 021032 (2017).
- [20] H. Ren, F. Pientka, S. Hart, A. T. Pierce, M. Kosowsky, L. Lunczer, R. Schlereth, B. Scharf, E. M. Hankiewicz, L. W. Molenkamp *et al.*, Topological superconductivity in a phase-controlled josephson junction, *Nature (London)* **569**, 93 (2019).
- [21] F. Setiawan, A. Stern, and E. Berg, Topological superconductivity in planar josephson junctions: Narrowing down to the nanowire limit, *Phys. Rev. B* **99**, 220506 (2019).
- [22] A. Stern and E. Berg, Fractional josephson vortices and braiding of majorana zero modes in planar superconductor-semiconductor heterostructures, *Phys. Rev. Lett.* **122**, 107701 (2019).
- [23] Z. Wang, J. O. Rodriguez, L. Jiao, S. Howard, M. Graham, G. Gu, T. L. Hughes, D. K. Morr, and V. Madhavan, Evidence for dispersing 1d majorana channels in an iron-based superconductor, *Science* **367**, 104 (2020).
- [24] P. Zhang, K. Yaji, T. Hashimoto, Y. Ota, T. Kondo, K. Okazaki, Z. Wang, J. Wen, G. Gu, H. Ding *et al.*, Observation of topological superconductivity on the surface of an iron-based superconductor, *Science* **360**, 182 (2018).
- [25] S. Kezilebieke, M. N. Huda, V. Vaño, M. Aapro, S. C. Ganguli, O. J. Silveira, S. Głodzik, A. S. Foster, T. Ojanen, and P. Liljeroth, Topological superconductivity in a van der Waals heterostructure, *Nature (London)* **588**, 424 (2020).
- [26] R. Aguado, Majorana quasiparticles in condensed matter, *Riv. Nuovo Cimento* **40**, 523 (2017).
- [27] J. Alicea, New directions in the pursuit of majorana fermions in solid state systems, *Rep. Prog. Phys.* **75**, 076501 (2012).
- [28] K. Flensberg, F. von Oppen, and A. Stern, Engineered platforms for topological superconductivity and majorana zero modes, *Nat. Rev. Mater.* **6**, 944 (2021).
- [29] M. Sato and Y. Ando, Topological superconductors: a review, *Rep. Prog. Phys.* **80**, 076501 (2017).
- [30] S. Ryu, A. P. Schnyder, A. Furusaki, and A. W. Ludwig, Topological insulators and superconductors: tenfold way and dimensional hierarchy, *New J. Phys.* **12**, 065010 (2010).
- [31] A. Haim and Y. Oreg, Time-reversal-invariant topological superconductivity in one and two dimensions, *Phys. Rep.* **825**, 1 (2019).
- [32] O. E. Casas, L. Arrachea, W. J. Herrera, and A. L. Yeyati, Proximity induced time-reversal topological superconductivity in Bi₂Se₃ films without phase tuning, *Phys. Rev. B* **99**, 161301 (2019).
- [33] E. Dumitrescu and S. Tewari, Topological properties of the time-reversal-symmetric Kitaev chain and applications to organic superconductors, *Phys. Rev. B* **88**, 220505 (2013).
- [34] H. Ebisu, B. Lu, J. Klinovaja, and Y. Tanaka, Theory of time-reversal topological superconductivity in double Rashba wires: Symmetries of cooper pairs and Andreev bound states, *Prog. Theor. Exp. Phys.* **2016**, 083101 (2016).
- [35] L. Fu and E. Berg, Odd-parity topological superconductors: theory and application to Cu_x Bi₂Se₃, *Phys. Rev. Lett.* **105**, 097001 (2010).
- [36] K. S. H. Kwon, and V. Yakovenko, Fractional ac josephson effect in p- and d-wave superconductors, *Eur. Phys. J. B* **37**, 349 (2003).
- [37] A. Haim, A. Keselman, E. Berg, and Y. Oreg, Time-reversal-invariant topological superconductivity induced by repulsive interactions in quantum wires, *Phys. Rev. B* **89**, 220504 (2014).
- [38] A. Haim, K. Wölms, E. Berg, Y. Oreg, and K. Flensberg, Interaction-driven topological superconductivity in one dimension, *Phys. Rev. B* **94**, 115124 (2016).
- [39] A. Keselman, L. Fu, A. Stern, and E. Berg, Inducing time-reversal-invariant topological superconductivity and fermion parity pumping in quantum wires, *Phys. Rev. Lett.* **111**, 116402 (2013).
- [40] J. Klinovaja, A. Yacoby, and D. Loss, Kramers pairs of majorana fermions and parafermions in fractional topological insulators, *Phys. Rev. B* **90**, 155447 (2014).
- [41] E. Mellars and B. Béri, Signatures of time-reversal-invariant topological superconductivity in the josephson effect, *Phys. Rev. B* **94**, 174508 (2016).
- [42] F. Parhizgar and A. M. Black-Schaffer, Highly tunable time-reversal-invariant topological superconductivity in topological insulator thin films, *Sci. Rep.* **7**, 9817 (2017).
- [43] X.-L. Qi, T. L. Hughes, S. Raghu, and S.-C. Zhang, Time-reversal-invariant topological superconductors and superfluids in two and three dimensions, *Phys. Rev. Lett.* **102**, 187001 (2009).
- [44] C. Reeg, C. Schrade, J. Klinovaja, and D. Loss, DIII topological superconductivity with emergent time-reversal symmetry, *Phys. Rev. B* **96**, 161407 (2017).
- [45] L. Santos, T. Neupert, C. Chamon, and C. Mudry, Superconductivity on the surface of topological insulators and in two-dimensional noncentrosymmetric materials, *Phys. Rev. B* **81**, 184502 (2010).
- [46] M. S. Scheurer and J. Schmalian, Topological superconductivity and unconventional pairing in oxide interfaces, *Nat. Commun.* **6**, 6005 (2015).
- [47] Y. Tanaka, Y. Mizuno, T. Yokoyama, K. Yada, and M. Sato, Anomalous andreev bound state in noncentrosymmetric superconductors, *Phys. Rev. Lett.* **105**, 097002 (2010).
- [48] C. L. Wong and K. T. Law, Majorana kramers doublets in $d_{x^2-y^2}$ -wave superconductors with rashba spin-orbit coupling, *Phys. Rev. B* **86**, 184516 (2012).
- [49] F. Zhang, C. Kane, and E. Mele, Time-reversal-invariant topological superconductivity and majorana kramers pairs, *Phys. Rev. Lett.* **111**, 056402 (2013).
- [50] A. A. Aligia and L. Arrachea, Entangled end states with fractionalized spin projection in a time-reversal-invariant topological superconducting wire, *Phys. Rev. B* **98**, 174507 (2018).
- [51] L. Arrachea, A. Camjayi, A. A. Aligia, and L. Grunheiro, Catalog of andreev spectra and josephson effects in structures with time-

- reversal-invariant topological superconductor wires, *Phys. Rev. B* **99**, 085431 (2019).
- [52] A. Camjayi, L. Arrachea, A. Aligia, and F. Von Oppen, Fractional spin and josephson effect in time-reversal-invariant topological superconductors, *Phys. Rev. Lett.* **119**, 046801 (2017).
- [53] L. M. Chinellato, C. J. Gazza, A. M. Lobos, and A. A. Aligia, Topological phases of strongly interacting time-reversal invariant topological superconducting chains under a magnetic field, *Phys. Rev. B* **109**, 064503 (2024).
- [54] S. B. Chung, J. Horowitz, and X.-L. Qi, Time-reversal anomaly and josephson effect in time-reversal-invariant topological superconductors, *Phys. Rev. B* **88**, 214514 (2013).
- [55] G. Francica, M. Cuoco, and P. Gentile, Topological superconducting phases and Josephson effect in curved superconductors with time reversal invariance, *Phys. Rev. B* **101**, 094504 (2020).
- [56] W.-J. Gong, Z. Gao, W.-F. Shan, and G.-Y. Yi, Influence of an embedded quantum dot on the josephson effect in the topological superconducting junction with majorana doublets, *Sci. Rep.* **6**, 23033 (2016).
- [57] A. Haim, Spontaneous josephson π junctions with topological superconductors, *Phys. Rev. B* **100**, 064505 (2019).
- [58] C. Knapp, A. Chew, and J. Alicea, Fragility of the fractional josephson effect in time-reversal-invariant topological superconductors, *Phys. Rev. Lett.* **125**, 207002 (2020).
- [59] L. Lauke, M. S. Scheurer, A. Poenicke, and J. Schmalian, Friedel oscillations and majorana zero modes in inhomogeneous superconductors, *Phys. Rev. B* **98**, 134502 (2018).
- [60] J. Li, W. Pan, B. A. Bernevig, and R. M. Lutchyn, Detection of majorana kramers pairs using a quantum point contact, *Phys. Rev. Lett.* **117**, 046804 (2016).
- [61] M. Mashkooi, A. Moghaddam, M. Hajibabaei, A. M. Black-Schaffer, and F. Parhizgar, Impact of topology on the impurity effects in extended s-wave superconductors with spin-orbit coupling, *Phys. Rev. B* **99**, 014508 (2019).
- [62] S. Nakosai, J. C. Budich, Y. Tanaka, B. Trauzettel, and N. Nagaosa, Majorana bound states and nonlocal spin correlations in a quantum wire on an unconventional superconductor, *Phys. Rev. Lett.* **110**, 117002 (2013).
- [63] C. Schrade and L. Fu, Parity-controlled 2π josephson effect mediated by majorana kramers pairs, *Phys. Rev. Lett.* **120**, 267002 (2018).
- [64] C. Schrade, A. Zyuzin, J. Klinovaja, and D. Loss, Proximity-induced π josephson junctions in topological insulators and kramers pairs of majorana fermions, *Phys. Rev. Lett.* **115**, 237001 (2015).
- [65] T. Pérez and A. A. Aligia, Effect of interatomic repulsion on majorana zero modes in a coupled quantum-dot-superconducting-nanowire hybrid system, *Phys. Rev. B* **109**, 075416 (2024).
- [66] Y. Volpez, D. Loss, and J. Klinovaja, Time-reversal invariant topological superconductivity in planar josephson junction, *Phys. Rev. Res.* **2**, 023415 (2020).
- [67] G. F. R. Ruiz, M. A. Rampp, A. A. Aligia, J. Schmalian, and L. Arrachea, Josephson junctions of two-dimensional time-reversal invariant superconductors: Signatures of the topological phase, *Phys. Rev. B* **106**, 195415 (2022).
- [68] A. Reich, E. Berg, J. Schmalian, and A. Shnirman, Magnetization dynamics and peierls instability in topological josephson structures, *Phys. Rev. B* **107**, 245411 (2023).
- [69] A. Barone and G. Paterno, *Physics and Applications of the Josephson Effect* (Wiley, New York, 1982).
- [70] J. Cuevas-Maraver, P. G. Kevrekidis, and F. Williams, *The Sine-Gordon Model and its Applications*, Nonlinear Systems and Complexity Vol. 10 (Springer, Cham, 2014).
- [71] E. D. J. Bergman, Y. I. Ben-Jacob, and K. Maki, Sine-gordon solitons: Particles obeying relativistic dynamics, *Phys. Rev. A* **27**, 3345 (1983).
- [72] Y. S. Kivshar and B. A. Malomed, Dynamics of solitons in nearly integrable systems, *Rev. Mod. Phys.* **61**, 763 (1989).
- [73] K. K. Likharev, *Dynamics of Josephson Junctions and Circuits* (CRC Press, Boca Raton, FL, 1986).
- [74] D. W. McLaughlin and A. C. Scott, Perturbation analysis of fluxon dynamics, *Phys. Rev. A* **18**, 1652 (1978).
- [75] A. Ustinov, Solitons in josephson junctions, *Phys. D (Amsterdam)* **123**, 315 (1998).
- [76] D. K. Campbell, M. Peyrard, and P. Sodano, Kink-antikink interactions in the double sine-gordon equation, *Phys. D (Amsterdam)* **19**, 165 (1986).
- [77] E. Grosfeld and A. Stern, Observing majorana bound states of josephson vortices in topological superconductors, *Proc. Natl. Acad. Sci. USA* **108**, 11810 (2011).
- [78] J. Goldstone and F. Wilczek, Fractional quantum numbers on solitons, *Phys. Rev. Lett.* **47**, 986 (1981).
- [79] R. Jackiw and C. Rebbi, Solitons with fermion number $1/2$, *Phys. Rev. D* **13**, 3398 (1976).
- [80] Z. Hermon, A. Stern, and E. Ben-Jacob, Quantum dynamics of a fluxon in a long circular josephson junction, *Phys. Rev. B* **49**, 9757 (1994).
- [81] A. A. Abdumalikov, G. L. Alfimov, and A. S. Malishevskii, Nonlocal electrodynamics of josephson vortices in superconducting circuits, *Supercond. Sci. Technol.* **22**, 023001 (2009).
- [82] M. Tinkham, *Introduction to Superconductivity*, Dover Books on Physics, 2nd ed. (Dover, New York, 2004).
- [83] T. Grover, D. N. Sheng, and A. Vishwanath, Emergent space-time supersymmetry at the boundary of a topological phase, *Science* **344**, 280 (2014).
- [84] A. Rahmani, X. Zhu, M. Franz, and I. Affleck, Emergent Supersymmetry from Strongly Interacting Majorana Zero Modes, *Phys. Rev. Lett.* **115**, 166401 (2015).
- [85] D. J. Gross and A. Neveu, Dynamical symmetry breaking in asymptotically free field theories, *Phys. Rev. D* **10**, 3235 (1974).
- [86] L. Grunheiro, M. Alvarado, A. L. Yeyati, and L. Arrachea, Transport features of a topological superconducting nanowire with a quantum dot: Conductance and noise, *Phys. Rev. B* **108**, 045418 (2023).
- [87] B. Altshul, Fermions in a multi-soliton background in $1+1$ dimensions, [arXiv:hep-th/0111042](https://arxiv.org/abs/hep-th/0111042).
- [88] V. G. Vaks, V. M. Galitskii, and A. I. Larkin, Collective excitations in a superconductor, *Sov. Phys.-JETP* **14**, 1 (1962).